Ejecta from impact craters

Kevin R. Housen [a,*], Keith A. Holsapple [b,c]

[a] Physical Sciences, MS 2T-50, The Boeing Co., P.O. Box 3707, Seattle, WA 98124, United States
[b] Planetary Science Institute, Tucson, AZ 85719-2395, United States
[c] University of Washington, Seattle, WA 98195, United States

ARTICLE INFO

ABSTRACT

An important feature of impacts into Solar System bodies is the fate of crater ejecta, the near-surface material launched during the highly dynamic crater formation process. Laboratory measurements of impact crater ejecta from 18 studies are summarized. The data are examined and used to assess our understanding of how the ejecta velocity and mass distributions depend on the conditions of an impact event. The effects of impact speed on the ejecta are reasonably well understood, but the dependences on target properties such as strength and porosity are only poorly constrained. A point-source scaling model for the ejecta mass and velocity distributions is developed and fit to the data for several classes of materials distinguished by porosity.

1. Introduction

Impact cratering has been a major factor in the geological evolution of the Solar System. The accompanying excavation and ejection of surface material is the process by which regoliths are formed and meteorite precursors escape from their parent bodies. It is essential to understand the mass and velocity distribution of the ejecta because those determine whether collisions are erosive or accretional, whether regolith materials are scattered widely or locally, whether blocks are retained on small asteroids, and so on.

Housen et al. (1983) constructed the basic framework for the scaling laws that describe ejecta velocity distributions and provided specific estimates based on the handful of data available at the time. In the ensuing 27 years, new techniques have been developed to measure ejecta velocities and a variety of ejecta velocity measurements have appeared in the literature.

In addition, significant new insights have been gained from spacecraft observations of asteroids. For example, the scaling law for rocky materials presented by Housen et al. (1983) and subsequently used by Veverka et al. (1986) indicated that rocky asteroids with diameter less than about 70 km should be barren.[1] This prediction was contradicted when substantial regoliths (Sullivan et al., 2002) were observed on small rocky asteroids such as Gaspra (12 km), Eros (15 km) and Ida (31 km). Clearly, our expectations for ejecta from impacts in rock needed to be revised (Housen, 1992).

Asteroid Mathilde, a 50 km body with perhaps 50% void space (Veverka et al., 1999), also gave impact modelers a wake-up call. Mathilde's large craters show no evidence of the substantial ejecta deposits that have always been observed around such structures, even on a body such as Phobos that is roughly half the size of Mathilde. Our experiments (Housen and Holsapple, 2003) suggest that material was not ejected from Mathilde's large craters because of its high porosity, but code calculations (Asphaug et al., 1998) concluded that nearly all of it escaped. In either case, Mathilde's craters underscore the importance of including porosity in considerations of ejecta velocities.

The purpose of this paper is to collect, summarize, and interpret the current knowledge of ejecta velocity distributions within the scaling theory, and to highlight areas that need further study. The next two sections define the terminology used and the scaling laws that apply to ejecta. Section 4 summarizes the sources of ejecta data used in the analysis. The data are then examined within the framework of the scaling laws in Section 5. Section 6 describes an ejecta model and provides fits to the data for various target materials.

2. The ejecta velocity distribution

At an impact site, the energy and momentum of the impactor are locally and rapidly transmitted into the impacted target body.

---

* Corresponding author.

E-mail addresses: kevin.r.housen@boeing.com (K.R. Housen), holsapple@aa.washington.edu (K.A. Holsapple).

[1] There was a misprint in Veverka et al. (1986, p. 354). The text should have indicated that the diameter threshold for escape of all ejecta was about 70 km and 20 km for rocky and icy bodies, respectively.
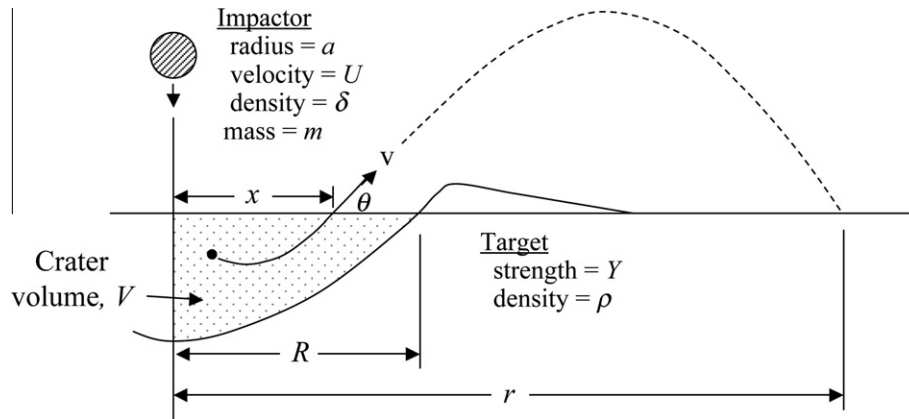
Fig. 1. Definition of variables.

The result is an expanding crater that is eventually arrested by either gravity or material strength. As the crater expands material is sheared, moving upward and outward along the crater bowl. The point at which a particle crosses through the original surface defines the launch position, x, and the ejection velocity, v, of the particle[2] (Fig. 1). When describing the ejecta velocity distribution, we often refer to the relationship between v and x without regard to the starting location of the particle. This is possible because particles that have the same surface launch position have very nearly the same launch velocity, even though the particles had a variety starting locations in the target.[3] This was shown experimentally by Piekutowski (1980), and confirmed in our own experiments and recent code calculations.

At least five different techniques have been used to measure the ejection velocity as a function of position, i.e. $v(x)$: (1) Piekutowski et al. (1977) measured velocities for small explosion events by using a sheet of light perpendicular to the target surface to illuminate a single plane of the ejecta plume. A camera with a rotating shutter recorded the positions of ejecta particles at discrete times, from which their trajectories could be determined. (2) Cintala et al. (1999) improved on this method by using a strobed laser and a CCD camera to record the trajectories. Once the trajectories were known, ballistic equations were used to determine the launch position, speed and angle. (3) An optical technique originally developed in the fluid mechanics community for visualization of flow fields was used by Schultz et al. (2000), Anderson et al. (2003), Anderson and Schultz (2005), and Hermalyn et al. (2009). In this method, images of a slice of the ejecta plume are acquired at different times. Rather than tracking specific particles in the plume, a cross-correlation analysis of image pairs is used to determine material motions after launch. (4) Piekutowski (1980) and Housen (2003) directly measured the *subsurface* material flow field, ejection velocity and position using a "quarter-space" technique in which a thick window was used as the front vertical face of the target container. The impact (or in some cases an explosion) occurred at a point along the target/window interface, which provided a cross-sectional view of the crater formation. Colored marker particles and high-speed films were used to track the material flow. (5) Screens or slotted plates have been used to mechanically isolate specific parts of the ejecta plume to facilitate velocity measurement from high-speed films (e.g. Oberbeck and Morrison, 1976; Yamamoto et al., 2005b).

Another way to quantify the ejecta velocity distribution is to define the total mass, $M(v)$, of material ejected with velocity greater than v. Because ejection velocities steadily decrease as the transient crater expands, the mass of material with velocity greater than v is also the mass of material having launch position less than the corresponding value of x.

Three methods have been applied to measurement of $M(v)$: (1) High-speed films have been used to directly measure the size and velocity of ejecta particles for rocky target materials (Gault et al., 1963; Housen, 1992). (2) The velocities of high-speed fine ejecta have been measured by placing thin witness foils around the periphery of the target (e.g. Yamamoto and Nakamura, 1997; Yamamoto et al., 2005a). The number and size of the holes and the known penetration relationships for the foils determined the mass of material with velocity greater than that needed to penetrate the foil. (3) The mass of material ejected to a given distance has been measured by placing ejecta collectors at various distances from the crater (e.g. Andrews, 1975; Stöffler et al., 1975; Hartmann, 1985; Michikami et al., 2007). An ejection velocity for each collector bin is calculated from the ejection angle (which is either assumed or estimated from high-speed imaging), along with assumptions about the launch position. $M(v)$ is then determined from the mass collected in each bin and the corresponding ejection velocities.

Ejecta experiments reported in the literature generally adopt one of the methods described above, and so provide direct measurements of either $v(x)$ or $M(v)$, but not both.[4] As a result, some target materials have more information on $v(x)$ than $M(v)$, or vice versa. In addition, the data were collected with varying impactor size, speed, target density, strength, etc. That data must be scaled in order to account for these differing conditions and to apply the data to the large-scale events of the Solar System. This is the purpose of ejecta scaling laws, discussed next.

3. Ejecta scaling laws

The scaling laws developed by Housen et al. (1983) for hypervelocity impact cratering were based on the experimentally verified fact that the projectile appears as a point source when considering any crater-related phenomena that occur very far from the impact point: it has even been observed to hold as close in as one projectile radius from the impact (Holsapple, 1993). Hence, the point-source concept applies to the final crater size, the growth of the transient crater and the majority of the observable ejecta field. We make use of this point-source concept here. For further details, the reader is

---

[2] In the ejecta model developed here, the velocity is a scalar quantity. Therefore, we use the terms velocity and speed interchangeably.

[3] But note that the time at which a particle crosses the surface does depend on its initial depth.

[4] A notable exception is Yamamoto et al. (2005b).

referred to Holsapple and Schmidt (1987) and Holsapple (1993).

At the heart of the point-source concept is the existence of a single measure, C, that entirely characterizes the impactor's influence on the cratering process in a given body. That measure must have the form

$$C = aU^\mu \delta^v \quad\quad (1)$$

where a, U, and δ are the impactor radius, velocity and mass density respectively. The power-law combination of those three impactor properties into one single governing measure is a consequence of the point source feature: there cannot be separate length or time scales (Holsapple, 1993). The point-source assumption is appropriate when the phenomena of interest occur at ranges greater than the impactor radius, and for impact velocities greater than the target sound speed, although there are important cases where its applicability is found to extend well inside those limits.

Data collected from the literature on cratering events in metals, and dry soils, and with a variety of impactor materials, shows that the exponent v on the mass density has the value of about 0.4 regardless of material type.[5] On the other hand, the exponent μ is known to depend on the high pressure properties of the target material, but must lie between the limits of momentum scaling, where $\mu = 1/3$, and energy scaling, where $\mu = 2/3$ (Holsapple and Schmidt, 1987). From many different experiments, $\mu \sim 0.41$ for dry soils and $\mu \sim 0.55$ for nonporous materials, such as water, metals, or rock. The value of μ for highly porous materials has not yet been determined, but is expected to be less than 0.4.

The point-source measure determines the outcome of an impact event in any given body. There are two different cases, depending on the event scale. Small craters in cohesive materials form in the "strength regime", because the bodies' material strength determines the crater size. For larger craters, gravity forces dominate any strength and thus gravity will determine the crater size. This is the "gravity regime".

The measure of strength, Y, deserves more discussion (Holsapple, 2009). There are many different strength measures of a material, e.g., compressive, shear (which involves the cohesion), tensile and others. In a metal, the compressive and tensile are about the same, and the shear strength is about ½ of those. But in a granular material, these strengths are not so easily related. The shear strength is about 2–3 times the tensile, and the compressive strength a factor of 5–20 times the tensile. Those ratios are determined by the angle of friction in the Mohr–Coulomb strength model. Thus, when scaling between materials with comparable angles of friction, one can use any of these strength measures and predict the same results. But when scaling to vastly different materials, that is not true. Since the cratering process in relatively low-porosity materials is dominated by shearing flow, perhaps the shear strength is the best to use for scaling. For highly porous materials, another strength determines the outcome: the "crush strength", i.e. the stress at which significant compaction of void space occurs. And finally, one should note that any strength scaling uses some strength with the units of stress. A cohesionless material such as dry sand has no such measure. Its strength, the result of shear resistance under confining pressure as described by the Mohr–Coulomb model, does not qualify as a "strength" for scaling

because it involves no material properties with units of stress: dry sand cratering follows gravity scaling at all event scales.

In each of the strength and gravity regimes, the scaling laws for ejecta can be cast in two forms, each of which has its advantages depending on the application of interest. For cases where the initial conditions of an impact are known but the final crater size is not (e.g. the Deep Impact event), it is useful to express the ejecta velocity distribution in terms of the impactor properties. In that form, the relations do not depend on the final crater size. On the other hand, if only the crater size is known, but not the impact conditions, then it is most convenient to express the scaling laws in terms of the final crater radius. This second case would arise when modeling the ejecta from, say, a given lunar crater for which the impactor size, velocity, etc. are unknown.

Because ejecta scaling relationships have been derived elsewhere, the full derivations are not presented here. Instead, the results are listed in Table 1 and an example is given that illustrates how the results are derived. Further information is provided by Housen et al. (1983) and Holsapple (1993).

Consider the ejection velocity versus position for an impact in the gravity regime. That velocity, v, is written as a function of the point-source measure, the target density ρ, surface gravity g, and launch position x:

$$v = f(aU^\mu\delta^v, \rho, g, x) \quad\quad (2)$$

This expression involves five quantities and three independent dimensional units and can therefore be written in terms of two nondimensional variables in various, but equivalent, ways. One such form is:

$$\frac{xv^\mu\rho^v}{aU^\mu\delta^v} = f\left(\frac{x(gx)^{\mu/2}\rho^v}{aU^\mu\delta^v}\right) \quad\quad (3)$$

which can be seen to be nondimensional and maintains the point source grouping of the impactor parameters. Rearrangement of this expression and taking the $1/\mu$ root gives the scaling law for the gravity regime:

$$\frac{v}{U} = \left[\frac{x}{a}\left(\frac{\rho}{\delta}\right)^v\right]^{-1/\mu}\hat{f}\left(\frac{x}{a}\left(\frac{ga}{U^2}\right)^{\mu/(2+\mu)}\left(\frac{\rho}{\delta}\right)^{2v/(2+\mu)}\right) \quad\quad (4)$$

where $\hat{f}(x) = f^{1/\mu}(x^{(2+\mu)/2})$. Although this scaling law can also be written in various other forms, we note that all are equivalent in the sense the fundamental dependence of ejection velocity on launch position, impact velocity, etc. does not depend on the particular form chosen.

Housen et al. (1983) noted that gravity should be important only for the furthest launch positions, which are near the crater edge. Inward from the edge, i.e. closer to the impact point, the kinetic energy associated with a particle in the excavation flow is large compared to both the work done against the gravity-induced shear strength of the target material and the change in gravitational potential energy incurred as the particle travels to the surface. Therefore, inward from the crater edge, the gravity-term in Eq. (4) should be insignificant and the scaling relation simplifies to

$$\frac{v}{U} = C_1\left[\frac{x}{a}\left(\frac{\rho}{\delta}\right)^v\right]^{-1/\mu} \qu\quad (5)$$

where C_1 is a constant to be determined from fits to data. As discussed below, the effect of gravity can be seen in some measurements of ejecta velocity, but the effect is usually small, and Eq. (5) provides a useful description of most of the ejecta field, until late in the flow.

If the flow were arrested by target strength rather than gravity, there would be a combination of terms with the strength on the right hand side of Eq. (4), but the strength would have also dropped

---

[5] The value of $v = 0.4$ is a consequence of the observation first made by Schmidt (1980) that for impacts into granular materials at a given value of the gravity-scaled impactor size ($\pi_2 = 3.22ga/U^2$), the cratering efficiency, defined as $\pi_V = \rho V/m$, is independent of the target or impactor density. Here, g is gravity, ρ is the target density, m is the impactor mass and V is the crater volume. The combination of the experiments reported by Schmidt (1980), as well as those reported by Schultz and Gault (1985) show this to be true for target/impactor density ratios varying by a factor of 1200. Additionally, Holsapple and Schmidt (1982) showed that $v = 0.4$ for impacts into metals. As a result, the value of v is quite well constrained.

Table 1
Scaling laws for the ejection velocity and crater size.

Crater radius		
Crater size	Strength regime : $R\left(\frac{\rho}{m}\right)^{1/3} = H_2 \left(\frac{\rho}{\delta}\right)^{(1-3\nu)/3} \left[\frac{Y}{\rho U^2}\right]^{-\mu/2}$	Gravity regime : $R\left(\frac{\rho}{m}\right)^{1/3} = H_1 \left(\frac{\rho}{\delta}\right)^{(2+\mu-6\nu)/[3(2+\mu)]} \left[\frac{ga}{U^2}\right]^{-\mu/(2+\mu)}$
Strength/gravity transition	$\frac{ga}{U^2} = \left(\frac{H_1}{H_2}\right)^{(2+\mu)/\mu} \left(\frac{\rho}{\delta}\right)^{\nu} \left(\frac{Y}{\rho U^2}\right)^{(2+\mu)/2}$	
Ejection velocity versus position		
In terms of impactor props.	$\frac{\nu}{U} = C_1 \left[\frac{x}{a}\left(\frac{\rho}{\delta}\right)^{\nu}\right]^{-1/\mu}$	
In terms of crater radius	Strength regime : $\nu\sqrt{\frac{\rho}{Y}} = C_3 \left(\frac{x}{R}\right)^{-1/\mu}$	Gravity regime : $\frac{\nu}{\sqrt{gR}} = C_2 \left(\frac{x}{R}\right)^{-1/\mu}$
	$C_3 = C_1 ((4\pi/3)^{1/3} H_2)^{-1/\mu}$	$C_2 = C_1 ((4\pi/3)^{1/3} H_1)^{-(2+\mu)/2\mu}$
Mass ejected from inside x	$M(x) = k\rho x^3$	
Mass ejected faster than v		
In terms of impactor props.	$\frac{M(\nu)}{m} = C_4 \left[\frac{\nu}{U}\left(\frac{\rho}{\delta}\right)^{\frac{3\nu-1}{3\mu}}\right]^{-3\mu}$	
	$C_4 = \frac{3k}{4\pi} C_1^{3\mu}$	
In terms of crater radius	Strength regime : $\frac{M(\nu)}{\rho R^3} = C_6 \left(\nu\sqrt{\frac{\rho}{Y}}\right)^{-3\mu}$	Gravity regime : $\frac{M(\nu)}{\rho R^3} = C_5 \left(\frac{\nu}{\sqrt{gR}}\right)^{-3\mu}$
	$C_6 = C_4 H_2^{-3}$	$C_5 = C_4 (4\pi/3)^{-\mu/2} H_1^{-3(\mu+2)/2}$

The symbols $C_1, \ldots, C_6$, H_1, H_2, and k are constants.

out when considering launch points inward from the crater edge using the same argument. Then we again would arrive at Eq. (5). Such a form is used below in Section 6. Thus, the form of the scaling law is the same in either strength or gravity-dominated impacts, but the range of x/a over which it holds will be shown to be different. The validity of this assumption will be tested when Eq. (5) is compared to laboratory data.

Now consider the form of the ejection velocity scaling law cast in terms of the final crater radius. In the gravity regime, the apparent radius, R, of the final crater is determined by some function

$$R = f(aU^\mu \delta^\nu, \rho, g) \qquad (6)$$

Using Eqs. (2) and (6) to eliminate the point-source measure gives the velocity in terms of the crater radius

$$\nu = f(R, \rho, g, x) \qquad (7)$$

The target density cannot occur in Eq. (7), because it is the only variable involving units of mass. The remaining four variables involve only the two independent dimensions of length and time, so there is a relation between two nondimensional variables:

$$\frac{\nu}{\sqrt{gR}} = f\left(\frac{x}{R}\right) \qquad (8)$$

which describes the ejection velocity at all launch positions for a gravity-dominated crater. There is an apparent dependence on the gravity g in this expression – in the left term and inherently in the crater radius R. But, as mentioned above, ν should not depend on gravity for launch points inward from the crater edge. The only way that this can occur in Eq. (8) is if the function f is a power-law in its argument so that the dependence of R on g cancels the square root of g on the left. The nondimensional form of Eq. (6) can be used to show that R is proportional to $g^{-\mu/(2+\mu)}$. As such, Eq. (8) is independent of g if and only if

$$\frac{\nu}{\sqrt{gR}} = C_2 \left(\frac{x}{R}\right)^{-1/\mu} \qquad (9)$$

which is easily verified with a little algebra. It should be noted that Eqs. (5) and (9) are entirely equivalent descriptions of the ejecta velocity distribution. The choice of which to use is a matter of which variables are known for a given problem: the impactor conditions or the crater size.

Using similar arguments, the scaling laws for $\nu(x)$ and for $M(\nu)$ can be determined. They are listed in Table 1 for both the strength and gravity regimes.

Note that the impact angle was not included in the above analysis. For oblique impacts, the ejecta fields need not be symmetric around the impact point: generally more high-speed ejecta will be launched down-stream (e.g. Anderson et al., 2003, 2004). That result is not precluded in the point-source assumptions, there is just a different point source solution for each impact angle, and the ejecta distributions will have an azimuthal angle dependence. Again, experiments are required to delineate the range for which that point-source result is valid (as discussed next), and specifically it may not hold for the earliest, highest-speed ejecta. But, it is known that many of the latest-stage results such as the final crater size and shape become simply related to the normal component of impact angle, and there is no observed asymmetry.

We make further comments about this case below.

3.1. Limits of applicability

When interpreting ejecta experiments, it is important to understand the conditions for which these scaling laws may apply. At and near the impact point, the point source does not apply and the scaling is separately dependent on δ, a and U (Holsapple, 1993). Consequently, distances scale with impactor radius a, velocities with U, pressures scale as δU^2, masses with δa^3 and so on. There is a cylindrical core in which no material is launched upwards: the material right under the impactor is driven down, and never remerges at the surface. The extent of that core depends on details such as the projectile shape and velocity. Therefore, the power-law forms based on the point-source measure shown in Table 1 must break down for small x. This is illustrated in Fig. 2. Part (a) of the figure shows that the point-source approximation holds only beyond some minimum distance which, for everything else fixed, is proportional to the impactor radius, i.e. $x = n_1 a$ where the multiplier n_1 depends on details such as impact speed, projectile shape, materials, and so on. More details are given below.

At greater distances from the impact, power-law scaling applies to the ejecta up to a distance near the crater edge, where the effects of gravity or strength arrest the flow to zero. Because this is the same mechanism responsible for determining the crater size, the location where the power-law breaks down is proportional to
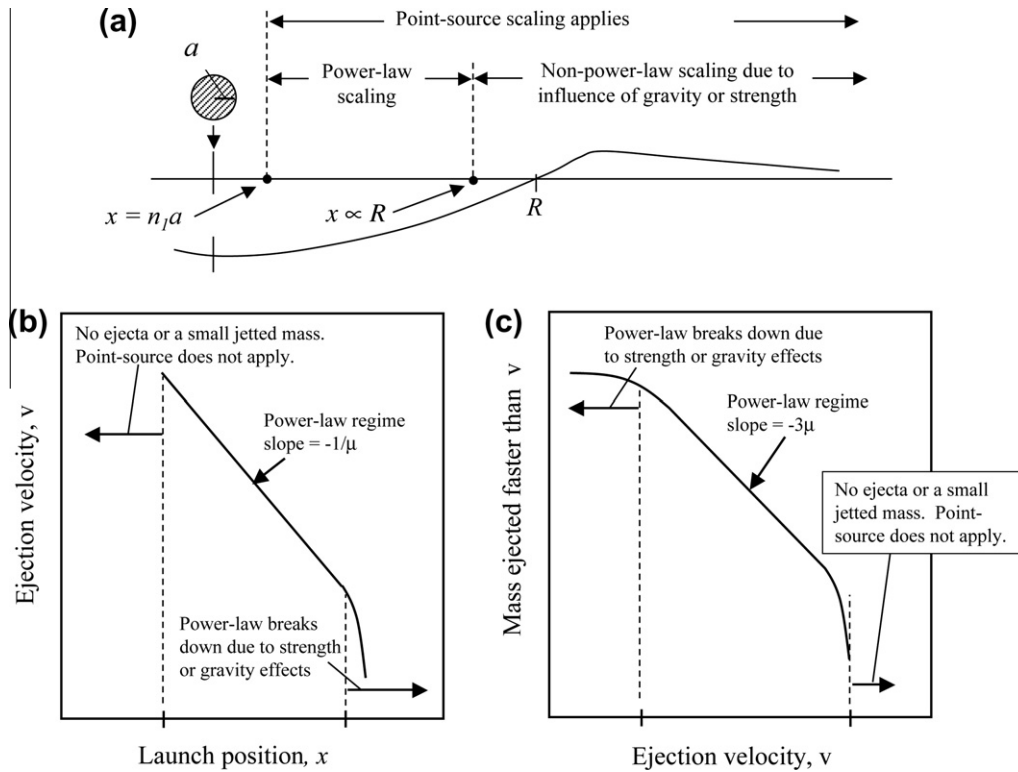
Fig. 2. (a) Point-source scaling only applies beyond some minimum distance from the impact. Power-law scaling holds from that point out to the location where gravity or target strength begin to arrest the cratering flow near the crater edge. (b) Schematic illustration of the behavior of the relation between ejection velocity and launch position. The highest velocities at the left are comparable to the impactor velocity. The middle portion of the distribution is a power-law, as expected from the point-source scaling analysis. At the right the cratering ceases and the velocities drop to zero. Part (c) shows the same behavior for the mass of material ejected to speeds greater than v. Here the maximum value on the ordinate is the total mass of ejected material, some fraction of the cratered mass.

the crater radius R. As discussed below, this proportionality constant is close to 1.

Fig. 2b shows the expected shape of the distribution of ejection velocity versus position on logarithmic axes. For small values of x, there is no ejecta, or it does not follow the power-law form. The power-law relationship given in Eq. (5) holds for the intermediate range of launch positions. Near the crater edge, the distribution must steepen because gravity or strength eventually stop the flow and all velocities approach zero.

Fig. 2c shows a similar behavior for the mass of ejecta with velocity greater than v. The high-velocity ejecta originate near the source, and the low velocity ejecta originate near the crater edge. The points that delimit the applicability of the power-law on this plot are shown as vertical dashed lines. At small values of the ejection velocity, the distribution flattens because of the effects of gravity or strength and approaches the total mass of ejected material.

Near the source, right at the projectile-body interface, a small mass of very high-speed material can be ejected by the "jetting" process (e.g. Yang and Ahrens, 1995). Jetting occurs when two surfaces collide at high speeds at a low angle. We ignore the jetting process here because it depends on details of the projectile shape and generally involves only a small mass of material. This is illustrated in Fig. 2b where the power-law terminates at the left end and in Fig. 2c where the curve approaches a vertical asymptote (ejecta mass goes to zero) at high ejection speeds.

Plots of $M(v)$ based on experimental data can turn downward from the power-law at high ejection speeds for another reason. The mass of fast ejecta is usually quite small and is therefore hard to observe in high-speed films, or to trap in collector bins due to the large ballistic ranges involved. In many laboratory experiments, the mass of the fast ejecta is a tiny fraction of a gram. Failure to collect even a small amount of this high-speed material can cause significant underestimation of $M(v)$ at large v. This is likely why it is common to see plots of $M(v)$ with slopes that are steeper than predicted by the scaling laws for large v.

Three additional important points should be made regarding the limits of power-law scaling. First, the regime of power-law scaling does not have sharply defined limits. That is, the effects of gravity or strength do not suddenly switch on beyond a specific point. However, as shown in the next section, the breakdown of the power-law is sufficiently rapid that it is reasonable to define an approximate region over which power-law scaling holds.

Second, the scaling of the ejecta velocity distribution can be expressed either in terms of the impactor properties, as in Eq. (5), or the crater size, as in Eq. (9). Note that one of the "end points" of the power-law regime depends on impactor size and the other end depends on crater size. As a result, one cannot construct a plot for all cases in which both end points are constant in a scaled sense. For example, consider a plot of $v(x)$ using the scaling given in Eq. (8). The largest distance that the power-law holds is proportional to R, so x/R is constant at that location. But the minimum distance for which the power-law holds is $x = n_1a$, or $x/R = n_1 (a/R)$. Therefore, the left-hand point at which the power-law breaks down written in terms of the crater radius depends on the ratio of impactor size to crater size for a given impact. In general then, one can expect the power-law to break down at various points for various datasets depending on the specific impact conditions. This is true for all plots of the ejecta velocity distribution, a point that is discussed further below.

Third, there are circumstances in which the power-law scaling regime can be minimal or even nonexistent. For example if the

impact velocity is very low, the crater may by only slightly larger than the projectile and the power-law regime shrinks to zero. Similarly, in gravity-dominated cratering, the crater edge forms relatively closer to the impactor in large events than in small events. Therefore, in sufficiently large events, the upper limit and the lower limit can squeeze together leaving little or no power-law region. This is included in the ejecta model described in Section 6.

4. Sources of ejecta data

The number of experimental measurements of impact crater ejecta velocity distributions has increased dramatically over the past two decades. Results reported in the impact literature were collected and are briefly summarized here. Each source of data is identified by a reference number, e.g. R1, R2, etc. Table 2 summarizes the data sources. The data are separated into measurements of $M(v)$ or $v(x)$, then further sorted in order of increasing target porosity. That same ordering is used in the summary given here.

4.1. Measurements of ejecta mass-velocity distribution

R1: Ejecta measurements for low-porosity materials are rare. Perhaps the most widely cited data are those of Gault et al. (1963), who impacted basalt at normal incidence with aluminum spheres at 6250 m/s. $M(v)$ was measured directly from high speed film records. Gault et al. interpreted the measurements of $M(v)$ at low ejection speeds as being upper limits because $M(v)$ exceeded the total crater mass, which is physically impossible. When plotted here, those data points are marked with arrows to indicate they are upper limits. Based on the crater mass, the points in question could not overestimate $M(v)$ by more than a factor of about 2–3.

R2: Housen (1992) used high-speed films to measure $M(v)$ for 1900 m/s impacts into weakly cemented basalt consisting of a mixture of mm-size crushed basalt fragments, iron grit (to achieve a desired bulk density), and fly ash as a binding agent. This material was designed as a simulant of large-scale jointed rock. An aluminum plate with a slot was suspended above the target surface. The plate allowed the impactor to pass through, but eliminated all but a single plane of ejected material. The sizes and trajectories (i.e. launch velocities) of the ejecta were determined from high-speed films. Two materials were used: a weak one having compressive and tensile strengths of 0.7 MPa and 0.09 MPa, and a stronger one with compressive and tensile strengths of 10 MPa and 0.45 MPa.

R3: Stöffler et al. (1975) fired Lexan cylinders into dry quartz sand targets at speeds of 6000–7000 m/s. They used catcher bins to measure the mass/area of ejecta as a function of range, r, from the impact point. $M(v)$ was obtained by an integration to find the mass ejected beyond range r, and by calculating the ejection velocity corresponding to each value of r. The ballistic equation relates the range and ejection velocity: $r = x + v^2\sin(2\theta)/g$, where θ is the launch angle (assumed to be 45°) and g is the gravitational acceleration. In this paper, two methods were used to calculate the launch velocity. In the first, all ejecta were assumed to be launched from the crater edge, $x = R$. This is obviously a good approximation for ejecta with $x \sim R$. Additionally, as noted by Hartmann (1985), it is also reasonable for material with $x \ll R$ because those ejecta have high speeds, so that the launch position is small compared to the v^2 term in the ballistic equation. Therefore, the calculated velocities are insensitive to the assumed launch position. The second method entails using a relation for $v(x)$ for sand to eliminate the launch position from the ballistic equation (see Housen et al. (1983) for details). The ejection velocities calculated from these two methods differed by only ~10% for the close-in ejecta and ~3% for the far-field ejecta. When plotting the data in a form normalized by the apparent crater radius, a value of $R = 12.7$ cm was used, based on a graphical estimation of the crater profiles presented by Stöffler et al.

R4: Yamamoto et al. (2005a) used polycarbonate projectiles to impact targets of loose soda-lime glass micro-spheres (236 ± 28 μm diameter) at a speed of ~240 m/s. They placed thin aluminum foils of various thicknesses around the periphery of the impact and then counted the holes left by ejecta penetrations. The areal density of holes along with a known relation between penetration velocity and foil thickness gave $M(v)$.

R5: Yamamoto et al. (2005b) also measured $M(v)$ for targets of loose glass micro-spheres (40 μm or 220 μm diameter) and polycarbonate projectiles (70–321 m/s). A slotted aluminum plate was placed over the target container to allow passage of material ejected in a single plane. Additionally, a partition was placed at a distance x from the impact, thereby deflecting ejecta with launch position less than x. A high-speed video camera was used to measure the speed of the ejecta just beyond the partition. By varying the placement of the partition, they measured $v(x)$. In a separate

Table 2
Sources of ejecta data.

Material	Porosity	Density (kg/m³)	Speed (m/s)	Crater	Reference
Measurements of M(v)					
Basalt	<few %	3000	6300	Strength	R1: Gault et al. (1963)
Weak. Cement. Basalt	23%	2600	1900	Strength	R2: Housen (1992)
Glass μ-spheres	36%	1500	240	Gravity	R4: Yamamoto et al. (2005a)
Glass μ-spheres	36%	1500	70–320	Gravity	R5: Yamamoto et al. (2005b)
Glass μ-spheres	36%	1500	190	Gravity	R6: Yamamoto et al. (2006)
Loose quartz sand	40%	1580	6800	Gravity	R3: Stöffler et al. (1975)
Basalt powder	43%	1700	7–2300	Gravity	R7: Hartmann (1985)
Sintered glass beads	7–80%	400–2300	1200–4500	Strength	R8: Michikami et al. (2007)
Perlite/sand	32–96%	100–1800	1800–2000	?	R9: Housen and Holsapple (2003)
Measurements of v(x)					
Water	0	1000	4.6	Gravity	R10: Schmidt and Housen (1987) and present work
Rock and alluvial soil	0–30%	–	–	–	R17: Perret and Bass (1974)
Dense Ottawa and	32%	1800	Explosion	Gravity	R11: Piekutowski (1980)
Dense Ottawa sand	32%	1800	1.9	Gravity	R12: Housen (2011)
Glass μ-spheres	38%	1600	2.0	Gravity	R12: Housen (2011)
Loose sand	40%	1600	1.0	Gravity	R13: Anderson et al. (2003)
Coarse sand	43%	1500	1.0	Gravity	R14: Anderson et al. (2007)
Coarse sand	43%	1500	0.8–1.9	Gravity	R15: Cintala et al. (1999)
Basalt gravel	43%	1400–1600	1.3	Gravity	R12: Housen (2011)
Perlite/sand	55–83%	400–1200	2.0	?	R16: Housen (2003, 2011)

experiment, the target was instead covered with an aluminum plate having a circular hole of radius x centered on the impact point. After an impact, they collected the mass of ejected material. They then calculated $M(v)$ from the measured mass of material ejected from inside x and the velocity of material at that launch position.

R6: Yamamoto et al. (2006) impacted glass micro-sphere (220 μm mean diameter) targets with polycarbonate projectiles at a speed of 192 m/s. Ejecta were collected in jars placed at various distances form the impact. Bounds on the ejection velocity associated with each collection jar were calculated from the range of ejection angles observed in video records and on the limiting cases of launch positions either at $x = 0$ or $x = R$.

R7: Hartmann (1985) impacted targets of loose basalt powder (800 μm median grain size) at speeds ranging from 7 m/s to 2300 m/s. He measured the mass of material ejected beyond a given range and estimated the ejection velocity for each range using the first method described above for the Stöffler et al. (1975) data. The total mass of ejecta was reported, as well as the fraction of ejecta with velocity greater than v. In the present analysis, those values were used to calculate $M(v)$.

R8: Michikami et al. (2005, 2007) explored the effects of target porosity and strength on the ejecta velocity distribution by constructing targets from sintered glass beads. The sintering process, and the addition of glass microballoons were used to produce target porosities between 7% and 80%. Alumina projectiles impacted the targets at speeds ranging from 1200 to 4500 m/s. The targets were attached to a vertical face of the impact chamber and were struck at normal incidence by the horizontally-moving projectile. Most of the ejecta produced in the experiments were observed to travel nearly perpendicular to the target surface (i.e. parallel to the floor of the chamber). Ejecta were collected in bins at various distances from the impact. The observed nearly-90° ejection angle and the fall-distance to the chamber floor were used to calculate the ejection velocity of material in the collection bins. The ejecta masses and velocities were used to calculate $M(v)$.

R9: Housen and Holsapple (2003) reported on impacts into porous materials made from mixtures of sand, Perlite (a porous silicate) and fly ash (a binding agent). The relative proportions of sand and Perlite were varied to obtain bulk porosities between 32% and 96%. The experiments were conducted on a geotechnic centrifuge, which simulates the formation of large-scale craters with diameters of tens of kilometers on asteroids.[6] Ejecta were collected on a thin cloth laid prior to the event around the anticipated periphery of the crater. For the present analysis, the ejection velocity needed to reach the ejecta collector was calculated by assuming that ejecta originated from the crater rim and were ejected at an angle of 45°. Thus each experiment yields the total mass of material ejected at speeds greater than that needed to reach the collector cloth. The experiments at various gravity (centripetal acceleration) levels provide data for different ejection velocities, because higher accelerations require higher ejection velocities to reach the collector.

The assumption that ejecta originated near the crater rim is justified because the edge of the collector cloth was close (typically 1–2 cm) to the crater rim. Thus, the slowest ejecta to reach the cloth would originate near the rim. The assumed ejection angle is consistent with laboratory measurements (e.g. Oberbeck and Morrison, 1976; Cintala et al., 1999). Furthermore, the calculated ejection velocities are insensitive to the ejection angle, θ. This results from the fact that the ballistic range is proportional to $\sin(2\theta)$, and 2θ in this case is close to 90°. For example, a variation of 5° in θ causes a variation in the ejection velocity of less than 1%.

4.2. Measurements of ejecta velocity versus launch position

R10: The only experimental measurement of $v(x)$ known to the authors for a zero-porosity material is from an impact test (shot 208Q) into water reported by Schmidt and Housen (1987). The impact occurred at 4600 m/s at normal incidence into a quarter-space test fixture with an ambient pressure slightly above the vapor pressure. Small plastic spheres placed on the water surface were tracked in high-speed films. Schmidt and Housen (1987) were primarily interested in crater growth and so did not measure ejection velocities. For the present analysis, the films were re-analyzed to measure $v(x)$ for the plastic tracer spheres. Examination of the films did not show any significant difference between the velocity of the spheres and the water ejecta.

R11: Piekutowski (1980) reported the first measurements of $v(x)$ for crater ejecta. His experiments used small explosive charges in a quarter-space fixture filled with dense Ottawa sand. Although this discussion is primarily about impact cratering, Piekutowski's results are included here because the shallow-buried charges he used are known to be good analogues of impact (Holsapple, 1980).

R12: One of the authors (KRH) has performed quarter-space impact experiments in targets of dense sand, of glass micro-spheres, of perlite/sand mixtures, and of basalt gravel. The impacts occurred at normal incidence, at speeds ranging from 1400 to 1900 m/s, and used polyethylene, magnesium, or aluminum cylinders as projectiles. The tests were conducted in a vacuum chamber at an ambient pressure of ∼10 mm Hg. Ejection velocities of colored marker particles were measured by tracking their trajectories. Additionally, the total mass of material ejected above a given speed was determined by associating a volume element of material with each tracer particle. The details of these experiments will be described in a separate paper (Housen, 2011).

R13: Anderson et al. (2003) used a particle image velocimetry (PIV) method to measure $v(x)$ for an impact of a 6.35 mm diameter aluminum sphere into loose sand (0.55 mm grain size) at an impact speed of ∼1000 m/s. The data were plotted in the form of $v/(gR)^{1/2}$ versus x/R and were converted for use here into v and x values by using an apparent crater radius of $R = 8.1$ cm (J. Anderson, personal communication).

R14: Anderson et al. (2007) measured $v(x)$ using the laser-based system of Cintala et al. (1999, see below). The targets were made from the 0.5–1 mm fraction of commercial blasting sand. The projectiles were soda-lime glass spheres, 3.18 mm in diameter, with speeds ranging from 320 to 1720 m/s. The data from a 1000 m/s impact were plotted and are used here. The launch positions were given in the form of x/R_r, where R_r is the "rim" radius of the crater measured from the impact point to the top of the rim. The reported crater size was used to calculate the launch position x. In the present analysis, these data are normalized by the apparent crater radius, R. The apparent radius is estimated by assuming that the ratio R_r/R is typically ∼1.3 (R.M. Schmidt, unpublished data).

R15: Cintala et al. (1999) used a strobed sheet of laser light to measure $v(x)$ for impacts of 4.76 mm diameter aluminum spheres into the 1–3 mm fraction of commercial blasting sand. The impact speed ranged from 800 to 1900 m/s. As in the discussion of Anderson et al. (2007) above, the reported rim radii were converted to apparent radii using $R_r/R = 1.3$.

R16: Housen (2003) described quarter-space impact experiments in porous targets made from mixtures of Perlite, quartz sand, and water. The targets, which were dried in an oven prior to testing, had a small cohesive strength as indicated by the ability of the material to support a vertical cliff of height 0.1 m cut into the material. Given that the cliff height was greater than the crater depth, the experiments were likely strength dominated. The material was too weak to be used in conventional compression or tensile tests. However, the lithostatic stress at the base of the

---

[6] The effects of gravity are measured by the gravity-scaled parameter ga/U^2, so increasing the gravity g produces the same physics as increasing the impactor size a.

vertical cliff, $\rho g h = 1000 * 9.8 * 0.1 \sim 1$ kPa provides a lower bound on the strength. An upper bound of 7 kPa is derived from a similar Perlite/sand mixture that used a small amount of binding agent. A nominal value of 2 kPa is used here for the tensile strength. The target porosity ranged from 55% to 67%. Colored tracer particles were used to measure $v(x)$ as the tracers passed upward through the original plane of the target surface.

R17: Perret and Bass (1974) reported material particle velocities from large underground nuclear explosions in rocks and alluvial soils. Although explosion experiments, those data provide useful information for low-porosity materials where impact data are rare.

5. Influence of impactor and target properties on the ejecta velocity distribution

In an ideal situation from the point of view of scaling, data would be available from ejecta experiments that include controlled variations of all variables that describe the impactor, the target, and ambient conditions. Although the literature now contains a relative abundance of ejecta data compared to the situation two decades ago, there are still significant holes in the database. For example, there are no experiments in which the impactor size is varied while holding all else constant. Additionally, it is very difficult, if not impossible, to independently vary the porosity, density, and strength properties of the target material. Nevertheless, many important aspects of scaling can be addressed using the current database.

When plotting data in a scaled form involving the crater size, the final size of the apparent crater (Fig. 1) is used. Literature data originally reported in terms of the rim radius are converted to apparent radius using a ratio of rim radius/apparent radius = 1.3, which is typically observed in these small impact experiments in cohesionless soils.

5.1. The effect of impact velocity

In the experiments reported by Cintala et al. (1999) for impacts into coarse sand, the impact velocity was varied from 800 m/s to 1.9 km/s while holding all else constant. Those results provide an excellent method to examine the effect of impact velocity on the ejecta velocity distribution $v(x)$. Fig. 3a shows the results from four of the experiments, plotted simply as launch velocity versus position. The data are ordered consistently in terms of impact velocity, i.e. the results for the lowest impact speeds have the lowest ejection velocity at a given launch position. Note also the apparent power-law behavior that extends to locations very near the crater radius (those radii are marked on the abscissa by small tics) indicating the range of the point-source assumption.

Fig. 3b shows the data in scaled form as per Eq. (5) and Table 1. In this form, the results for the various impact velocities collapse into a single trend, to within the scatter inherent in the measurements. In addition, the trend is well described as a power-law. The significance of these two observations is now discussed.

The collapse of the data onto a single trend in Fig. 3b is noteworthy because it shows that the scaling analysis did not exclude an important variable. Suppose, for example, that a variable such as the wave speed, c, of the target material had a significant effect on ejection velocity. Then in nondimensional form, $v/U = f(x/a, \rho/\delta, c/U)$ which allows an additional dependence on the impact velocity via the c/U variable. The data in Fig. 3b show that v/U is simply a function of x/a and ρ/δ with no additional dependence on impact speed U. Therefore, for these data[7] the function f does not depend
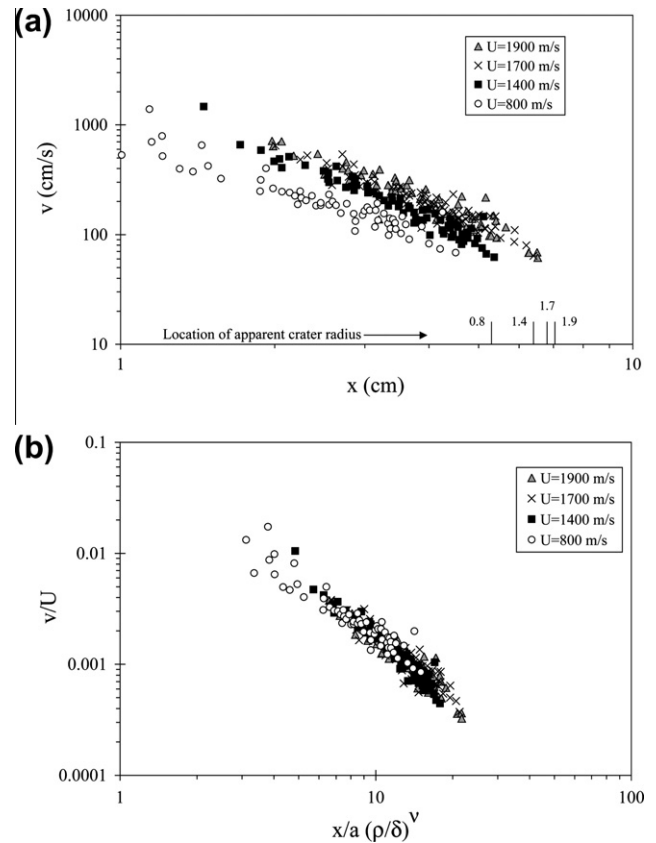

Fig. 3. Ejecta velocity measurements from Cintala et al. (1999) for dry sand, a gravity-dominated material. (a) Data for four impact velocities, plotted simply as ejection velocity versus launch position. The crater rim for each experiment is shown by a small tic on the abscissa, with each tic labeled by the impact velocity in km/s. (b) The same data but plotted in scaled form that correlates the results for different impact speeds.

on wave speed, and v is independent of c. This argument can be extended to any variable whose units involve time.

A similar argument can be made about other variables. If there were a dependence on the grain size, s, of a soil, the scaling relation for ejecta velocity would be $v/U = f(x/a, \rho/\delta, s/a)$. Variations in the impact velocity alone would not provide any information on the effect of s because the term s/a would be fixed. Instead, one would need to vary either the grain size or the impactor radius while holding all other (nondimensional) variables constant. The subject of grain size is addressed in Section 5.5.

The experiments of Hartmann (1985) into basalt powder also provide an interesting look at the effect of impact velocity because, even though the projectile size and type were not held constant, the impact velocity varied by more than a factor of 400. Fig. 4 shows his results for the mass distribution in scaled form, along with those into dry sand of Stöffler et al. (1975). Each dataset shows the behavior described in Section 2. For example, consider the results for shot 256, an impact at 2321 m/s. For the slower ejecta speeds, the data follow the expected power-law slope for a granular material with $\mu = 0.41$ (the value for dry sand). Moving toward higher ejecta speeds, the data trend steepens and then terminates at the speed corresponding to the largest distance that ejecta could be collected. In films of his experiments, Hartmann (1985) observed high-speed ejecta that could not be collected because it was moving at speeds several times greater than that needed to reach the most distant collector. As a result, $M(v)$ was underestimated at the high-speed end of each dataset shown in Fig. 4. Thus, the steepening of the data at high ejection speeds is at least

---

[7] The wave speed in sand is typically of order 100 m/s. Thus, even the slowest impact shown in Fig. 3 is several times larger than the target wave speed. One cannot use these data to rule out a dependence on c at much lower impact speeds.
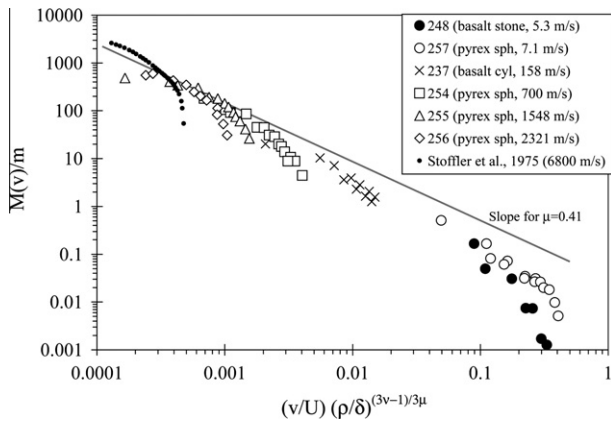
Fig. 4. Measurements of the mass of ejecta with speeds exceeding a value v from impacts into basalt powder (Hartmann, 1985) and dry quartz sand (Stöffler et al., 1975). Each dataset follows the general behavior illustrated in Fig. 2c, i.e. a power-law slope at low ejection speeds with a steeper slope at high speeds.

partially due to this uncollected high-speed material. If a sufficiently large test chamber were available, the data would be expected to follow along the downward power-law slope until reaching ejecta speeds where the point-source measure breaks down.

All of the data with impact velocity above 158 m/s are consistent with the power-law slope corresponding to $\mu = 0.41$, although the results for the three slowest tests fall below that trend. Shots 248, 257 and 237 were all at or well below 158 m/s, which is comparable to the sound speed in sand. Thus, an additional dependence on c/U could be expected and be responsible for the deviation from the power-law. Moreover, for shots 248 and 257 the total mass of ejecta was less than one impactor mass and the ejecta velocities approach the impact velocity. Clearly, the crater was not large compared to the impactor. As noted in Section 2, the point-source measure is not expected to apply in that case and the curve should steepen as v/U approaches one, consistent with the behavior shown in Fig. 4.

5.2. Impact angle

The angle between the projectile trajectory and the impacted surface can have an important effect on the cratering and ejection process. Although some progress has been made in studying oblique impacts, the data available at the time of this writing are not sufficient to develop a comprehensive model that includes impact angle, especially for highly oblique impacts. Therefore, the primary case considered here is that of normal, or nearly normal impact angles. Nevertheless, some qualitative observations can be made based on the current data.

Gault and Wedekind (1978) performed oblique impact experiments in particulate targets and found that the craters were circular as long as the impact angle was greater than about 30° from the target surface. Although ejecta distributions were not measured, this suggests that the late-time cratering motions are not strongly influenced by impact angles greater than 30°. Lower speed experiments with basaltic sand produced circular craters for impact angles greater than about 20° with respect to the target surface (Hessen et al., 2007). Although the craters were circular, Hessen et al. noted some asymmetries in the ejecta blanket for impact angles as high as 60°.

Direct measurements of the ejecta velocity distribution for 30° impacts in sand were reported by Anderson et al. (2003). Their results showed a significant dependence of ejection velocity on azimuth. Similar results for 30° impacts were reported by Hermalyn et al. (2008).

Yamamoto et al. (2006) measured ejecta velocity distributions for oblique impacts (192 m/s) in glass micro-spheres. They found $M(v)$ to be insensitive to impact angle as long as the angle was greater than 45° from the target surface. Interestingly, when $M(v)$ was plotted in scaled form in terms of the crater radius (bottom right cell of Table 1), the velocity distribution showed no discernable dependence on impact angle. Evidently, the crater radius accounted for the effect of variations in impact angle, and it is thought to scale with the normal component of the impact speed. Note, however, that Yamamoto et al. (2006) only measured the low-speed ejecta, i.e. the material deposited within several crater radii. Measurements of the high-speed ejecta (Yamamoto et al., 2005a) showed a significant dependence on impact angle, even when plotted in the form scaled by the crater radius.

So, it is apparent that the highest-speed ejecta has a definite dependence on the impact angle and is asymmetric. The later-stage, lower speed contributions, and the final crater size, may be symmetrical even for relatively low impact angles, and may scale just as a normal impact, but using the normal component of impact speed. Somewhere in between, at some intermediate ejecta velocities, there is the transition from an angle dependence to no dependence. Quantification of these possibilities awaits more data and analysis.

5.3. Projectile density

There are very few ejecta experiments in which the projectile density was varied while holding all other variables constant. In experiments to be reported elsewhere (Housen, 2011), quarter-space targets made from dry dense F75 Ottawa sand (200 μm median grain size, 1790 kg/m³ bulk density) were impacted by polyethylene (δ = 930 kg/m³), magnesium (1790 kg/m³), and aluminum (2780 kg/m³) cylinders. The impact velocity varied from 1400 to 1900 m/s. As shown in Fig. 5a, the factor of 3 variation in impactor density had a noticeable effect on ejecta velocities, even after the differences in impact velocity are accounted for. As shown in Fig. 5b, inclusion of the density ratio in the scaling with, v = 0.4 determined from impact crater size, does a reasonable job of correlating the results for the different projectile densities. However, additional experiments should be conducted to further understand how projectile density affects the ejecta velocity distribution.

5.4. Target strength

A significant influence of target strength, Y, on ejecta velocities can be seen by comparing experiments in solid basalt (Gault et al., 1963), weakly cemented basalt gravel (Housen, 1992), and sintered glass beads (Michikami et al., 2007). Fig. 6 shows these data in the form scaled by the impactor properties. Unfortunately, variations in target strength are usually accompanied by variations in target porosity, so it is difficult to separate the effects of these two variables. The experiments on weakly cemented basalt are an exception because the cementitious binder (fly ash) is a minor constituent in the target material. Therefore, strength can be varied without significantly changing porosity.

Consider first the data for weakly cemented basalt. Two targets were impacted, one with a static compressive and tensile strength of 0.7 MPa and 0.09 MPa and one with a compressive and tensile strength of 10 MPa and 0.45 MPa. Both targets had a porosity of 23 ± 1%. The general shape of the ejecta distribution is seen to be consistent with that described in Fig. 2c. There is a power-law region in which both data curves coalesce: there the velocity distribution is insensitive to material strength. It is difficult to estimate the scaling exponent μ from these data, but $\mu = 0.41$ is quite plausible as indicated by the line in the figure. Moving toward higher speeds, the distribution tends to steepen. This could be due to an inability to
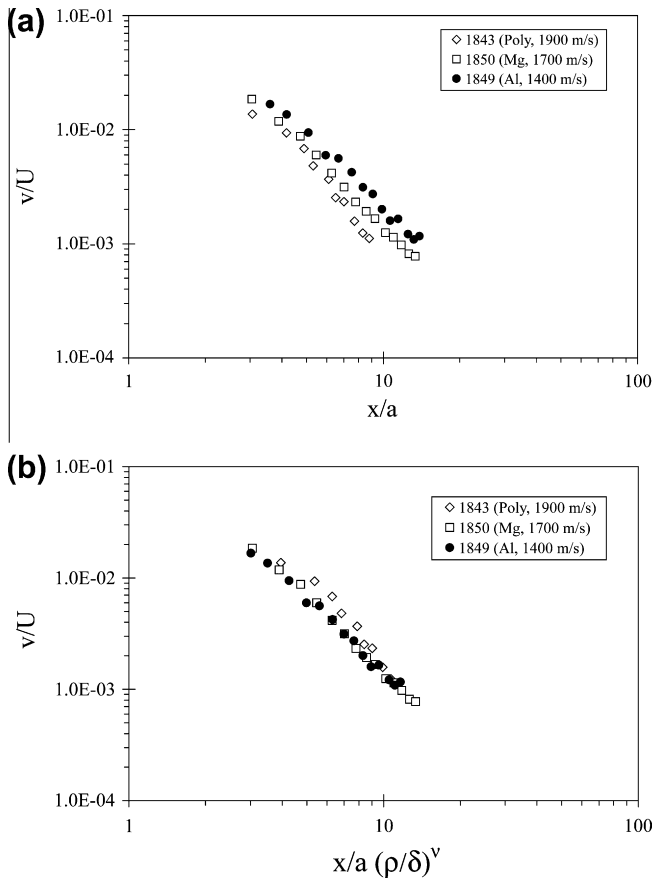
Fig. 5. Effect of projectile density on ejection velocities for impacts in dry sand (Housen, 2011). Parts (a) and (b) show the results before and after applying the point-source scaling to account for density variations.
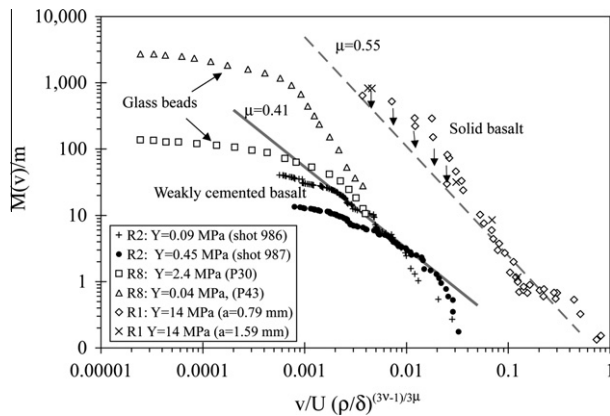

Fig. 6. Ejecta velocity distributions for strength dominated targets. The data for moderately porous materials (sintered glass beads and weakly cemented basalt) are separated at the low ejection velocities, where target strength determines the total ejecta mass, but coalesce at the higher ejection velocities, where strength effects are not too important. The data for solid basalt lie well above the other data because the low porosity of the basalt results in enhanced energy coupling into the target.

observe the high-speed ejecta, or to the expected breakdown of the point-source measure for points close to the impact. Moving back to low ejection velocities, the power-law breaks down due to the effects of target strength as $M(v)$ asymptotically approaches the total ejecta mass. Here the strength does matter because the weaker material ejects a greater mass.

Scaling laws can be used to show that the asymptotic (small v) value of $M(v)/m$ is proportional to $(\rho U^2/Y)^{3\mu/2}$. This in fact is the

scaling relation for final crater volume and merely states that the total ejecta mass is proportional to the "crater mass". For the weakly cemented basalt targets, both the impact velocity and target density were constant (1900 m/s, 2600 kg/m³). Therefore, the target with the higher strength should have a lower asymptotic value of $M(v)/m$, as observed. This is consistent with the fact that the stronger target exhibited a smaller crater and a correspondingly smaller total mass of ejecta.

The data for sintered glass beads show a behavior similar to the weakly cemented basalt. Fig. 6 shows results for two glass-bead targets: one with 30% porosity and 0.45 MPa tensile strength and one with 43% porosity and 0.04 MPa tensile strength. The effects of strength and porosity are hard to separate in these data because neither variable was constant. Nevertheless, the data coalesce at the higher ejecta velocities, where strength should not be important (note they also coalesce with the weakly cemented basalt). At low ejecta velocities, both of the glass-bead materials approach horizontal asymptotes with the weaker material lying above the stronger, as expected.

Although the data for glass beads and for weakly cemented basalt are internally consistent in that the weaker material within a given dataset lies above the stronger, there is an inconsistency between the two datasets. The unfilled square data points in Fig. 6 represent the glass bead target that had a porosity of 30%, which is not too far from the 23% of the weakly cemented basalt. However, the tensile strength (2.4 MPa), density (1800 kg/m³) and impact velocity (~4100 m/s) for the sintered glass result in a value $\rho U^2/Y$ that is a factor of 1.7 times smaller than for the 0.45 MPa weakly cemented basalt target (solid circles in Fig. 6). Therefore, the asymptotic value of $M(v)/m$ for the glass beads should be lower than the weakly cemented basalt. Fig. 6 shows that the asymptote is instead about an order of magnitude *larger*. This discrepancy is hard to explain based on any strength measure. However, we note that the glass-bead targets were oriented with a vertical surface, and the projectile impacted horizontally. Thus any material broken from the shock would just fall from the target, and would not be ejecta in the usual sense.

The results for solid basalt targets lie significantly above and to the right of those for the sintered glass beads or the weakly cemented basalt gravel.[8] This is most likely due to the lower porosity of the solid target, which results in much better coupling of the impact energy and momentum. Lower porosity is also associated with larger μ, thus resulting in a steeper slope for the solid basalt compared to the other materials in Fig. 6. Given the uncertainties in the data at the low-velocity end of the distribution, the solid basalt data are roughly consistent with the expected value of $\mu = 0.55$.

The variations due to target properties can largely be removed by normalizing the data by the crater size, target density and (tensile) strength. This is shown in Fig. 7 in which the data have been plotted in the scaled form shown in Table 1 for the strength regime. The weakly cemented basalt results fall on a common trend about which the remaining data tend to cluster. The results for sintered glass beads show a trend similar to the other datasets, i.e. a power-law at the higher ejection velocities that flattens out at the lower velocities, as expected due to the increasing effects of target strength near the crater edge.

The consistency of the data shown in Fig. 7 is remarkable given that the target strength varies by a factor of ~350 and the porosity varies from near-zero to 43%. Evidently, the various effects of target strength, density, porosity, and impactor properties are encapsulated in the crater size. It is interesting to note, however, that the

---

[8] The data for solid basalt at low ejection velocities are shown with downward pointing arrows because, as noted by Gault et al. (1963), measurement uncertainties resulted in $M(v)$ unrealistically exceeding the crater mass at the low-velocity end of the distribution.
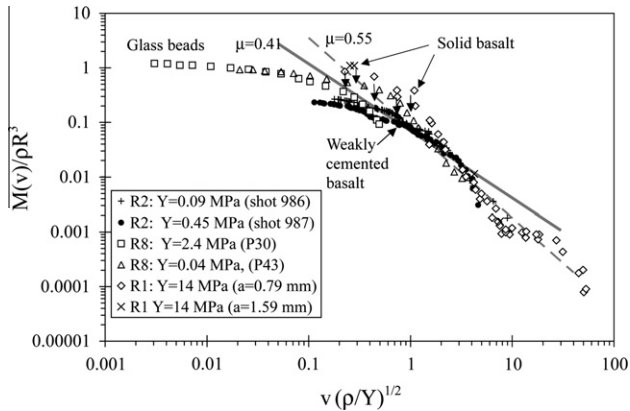
Fig. 7. The data shown in Fig. 6 are collapsed onto a common trend by plotting the data in the form involving crater radius.

data for solid basalt show a steeper trend than do the data for other, more porous materials. As discussed in Section 3 and as shown in Table 1, $M(v)$ is proportional to v to the power -3μ. Target materials with the lowest porosity have larger values of μ, which is consistent with the steep slope exhibited by the data for (low porosity, high μ) solid basalt.

To first order, the data indicate that the power-law trend breaks down when the scaled ejection velocity $v(\rho/Y)^{1/2}$ is less than approximately one, i.e. when the "dynamic pressure" of the ejecta ρv^2 is about equal to the target strength Y. This condition has been used in the past to define a minimum, or cutoff ejection velocity for strength-dominated impacts, i.e. a non-zero ejection velocity at the crater rim (e.g. Richardson et al., 2005). However, instead of displaying a sharp cutoff, the velocity distribution is observed to gradually flatten down to velocities at least two orders of magnitude below the presumed cutoff. Note also that the majority of the ejecta mass is in this low-velocity range so one cannot use that cutoff to estimate the ejected mass. It is clear that much more needs to be done in order to understand the effects of target strength, in particular in identifying the appropriate measure of strength.

5.5. Grain size

For impacts into fine-grained sands and for large-scale events, the projectile, and thus the width of the stress pulse, is typically much larger than the constituent grains. In this case the target material is approximated as a continuum. On the other hand, if the projectile is comparable to or smaller than the typical grain, the grain size could have a significant effect on the energy and momentum coupling and distribution and on the subsequent crater growth, material ejection, and so on. This possibility has been noted in several studies, e.g. Cintala et al. (1999), Barnouin-Jha et al. (2002) and Anderson et al. (2007).

Cintala et al. (1999) reported on experiments in which 4.76 mm diameter aluminum spheres impacted coarse sand targets with grain diameters in the range of 1–3 mm. The values of μ determined from the ejecta velocity distribution $v(x)$ were all larger than the value of μ determined from the dependence of crater size on impact velocity. They attributed this to the fact that the ratio, ψ = projectile diameter/grain diameter, was only ~2.7. Anderson et al. (2007) used the same ejecta velocity measurement method as Cintala et al. (1999) and found a similar result when they impacted sand targets with ψ = 4.5. But for relatively finer grains (ψ = 11.5), Anderson et al. (2004) used a PIV method to measure ejection velocity and found consistent values of μ. If grain size is the reason for the inconsistent values of μ, these results suggest that ψ should be at least 5 or 10 for the grain size effect to vanish.

The effect of grain size was also investigated in experiments by one of the present authors (KRH). Fig. 8 shows the results of four quarter-space experiments in which 12 mm (dia) × 12 mm (high) aluminum cylinders impacted granular targets at 1000 m/s. The impacts occurred at normal incidence in a vacuum chamber. One of the targets was F75 sand, with a median grain diameter of 0.24 mm. The other three experiments used basalt gravel with median grain sizes of 1.3 mm, 9.5 mm, and 38 mm. Overall, ψ ranged from 50 (F75 sand) down to 0.32 for the coarsest gravel. The inset on the right side of Fig. 8 illustrates the basalt gravel targets prior to impact, with the white rectangle showing the size of the projectile and the point of impact.

High-speed videos of the events were used to measure the velocity of ejected grains as a function of their launch position. Surprisingly, the results from the F75 sand and the two finest basalt gravel targets agree very well. Thus, everything else being equal, the granularity of the target apparently did not have a significant effect on the ejecta velocity distribution in these experiments even for ψ as small as 1.3 (shot 3674).

As shown in the bottom segment of the inset in Fig. 8, the impact on the coarsest target (shot 3649) occurred on a gravel fragment that was a few times larger than the projectile. The dust generated in this super-catastrophic collision obscured much of the video, so only one ejected fragment could be reliably measured. Furthermore, it is possible that the result of shot 3649 may have been quite different had the projectile hit between fragments. Nevertheless, this single data point agrees well with the results from the finer targets.

Although further work should be done to verify the results given in Fig. 8, the velocity distribution even for very lumpy targets may be quite close to that for fine-grained materials. If this is true, then some other factor (e.g. material property or initial conditions) must be responsible for the observations of Cintala et al. (1999).

5.6. Grain shape

The shapes of grains in granular materials could have an important effect on ejecta because shape determines the amount of grain interlocking which governs the resistance of the material to shearing deformations. Thus, granular materials such as coarse angular sands tend to have higher angles of internal friction, and correspondingly higher shear strengths when confined with pressure, than do materials composed of smooth spherical particles. Comparing impacts into dry sand with impacts into glass micro-spheres provides a good test of the effects of grain shape because both
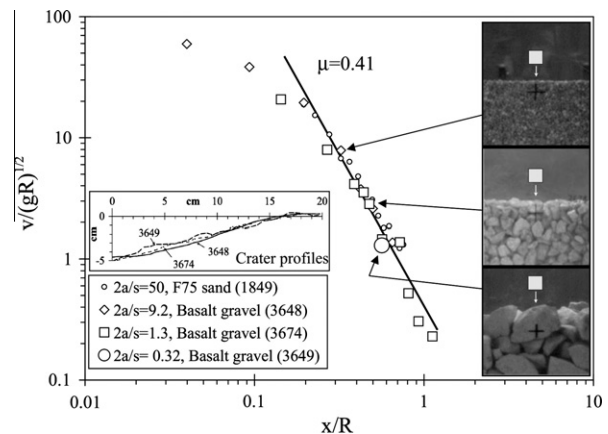

Fig. 8. Results of impacts into fine and coarse granular materials. Variation in the ratio of projectile diameter (2a) to grain diameter (s) from 50 down to 0.32 had only a minor effect on ejection velocities or crater profile.

materials have comparable mineral compositions, bulk densities and porosities. However, the angular shapes of sand grains produce an angle of internal friction of ∼30–40°, while that for glass spheres is ∼20°.

Fig. 9 compares ejecta velocity measurements for dry sand and glass micro-sphere targets using the scaling form in terms of the impactor properties. The sand data cluster along a power-law trend. The data for glass micro-spheres reported by Yamamoto et al. (2005b) lie about a factor of 3 above the dry sand data. This suggests that the low friction angle (low shear strength) of the glass spheres causes an increase in ejection velocity at a given position. On the other hand, the solid black square symbols (Housen, 2011) in the figure are also for glass micro-spheres and agree quite well with the dry sand data.

The main difference between the two sets of data for micro-spheres is that the impact velocity of 1800 m/s for the Housen (2011) experiments is considerably larger than the 70–320 m/s used in the experiments reported by Yamamoto et al. (2005b). Recall from the discussion in Section 5.1 that the scaling accounts for variations in the impact velocity. However, if the target wave speed is important (which is expected when the impact velocity is comparable to or less than the target sound speed), the velocity distribution need not be a simple power-law. Measurements reported by Teramoto and Yano (2005) indicate that the wave speed for glass spheres is between 100 and 200 m/s. Therefore much of the Yamamoto et al. (2005b) data were from sub-sonic impacts, which may be responsible for the discrepancy between the two sets of data for micro-spheres shown in Fig. 9. At lower impact speeds there is less energy dissipation, resulting in relatively larger craters and ejection velocities. But the effect of grain shape or friction angle on ejection velocity remains unclear at present. This question could be addressed by performing a controlled set of experiments in micro-spheres over a larger range of impact velocities, especially the higher ones.

Indeed the Yamamoto et al. (2005b) experiments not only produced ejection velocities higher than for sand, they also produced larger craters. As a result, when plotted in terms of crater size, all of the ejecta data for micro-spheres agree much better with that of sand. This is shown in Fig. 10. Therefore, regardless of which factor (friction angle, wave speed, etc.) was responsible for the high ejection velocities in the Yamamoto et al. (2005b) experiments, normalizing the data by the crater radius accounts for this effect and does a better job of collapsing the data onto a single power-law trend. Stated another way, whatever the cause (a material property, the sub-sonic impacts, energy dissipation, etc.), it affected the crater size and ejecta characteristics in the same way.

5.7. Target porosity

As noted earlier, isolating the effects of target porosity is challenging because of difficulties in varying porosity without simultaneously varying other mechanical properties, such as strength. Nevertheless, useful comparisons can be made, and an example is shown in Fig. 11. Data for ejection velocity versus position are shown for dry sands, with porosities of 30–40%, and for three mixtures of porous silicate (Perlite) and sand, whose bulk porosities were 55%, 67% and 83%. The ejecta velocities for the 55% and 67% porous materials are distinctly lower than those for dry sand, by as much as a factor of 2 near the crater edge. This velocity reduction is not surprising given the energy losses that occur as the impact shock crushes the pore spaces, especially near the impact point where energy and momentum coupling occur. Additionally, a regression to these data (excluding the points at the high ejection velocities, where the point-source approximation breaks down) gives a value of $\mu = 0.35$, which follows the expectation that increased porosity corresponds to values of μ closer to the momentum scaling limit of 1/3. The data for 83% porosity show an even more dramatic reduction of ejection velocity compared to dry sand.

Fig. 11 also shows that the ejection velocities for water are considerably above and to the right of the data for sand. The comparison with granular materials is complicated by the fact that the porosity and the friction angle of water are both zero. Nevertheless, the relatively high velocities for water are likely due to its low porosity, which results in efficient coupling of the impact energy
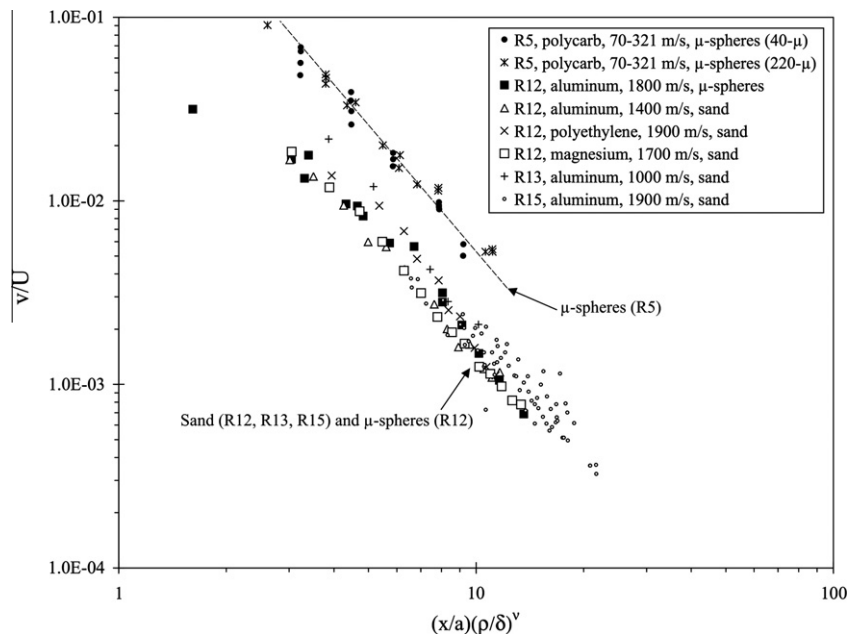

Fig. 9. The shape of grains in a granular material determines its resistance to shear (friction angle) and could therefore affect ejection velocities. Data for glass micro-spheres (Yamamoto et al., 2005b, labeled as R5), with a friction angle of ∼20°, lie significantly above those for dry sands, whose friction angle is 30–40°. However, data for glass micro-spheres from Housen (2011, labeled R12) agree with the dry sand data. As discussed in the text, the reason for this difference is not yet clear. The legend lists the projectile material, impact speed and target material for each dataset.
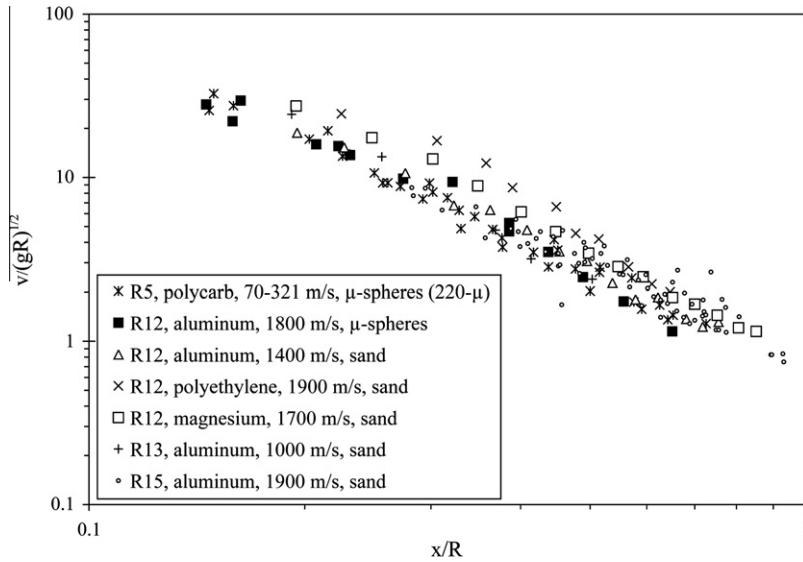
Fig. 10. The data in Fig. 9 are collapsed onto a common trend by plotting the data in the scaling form that involves crater radius. The apparent crater radius for 220μ microspheres (R5) was provided by Yamamoto (personal communication, 2009).
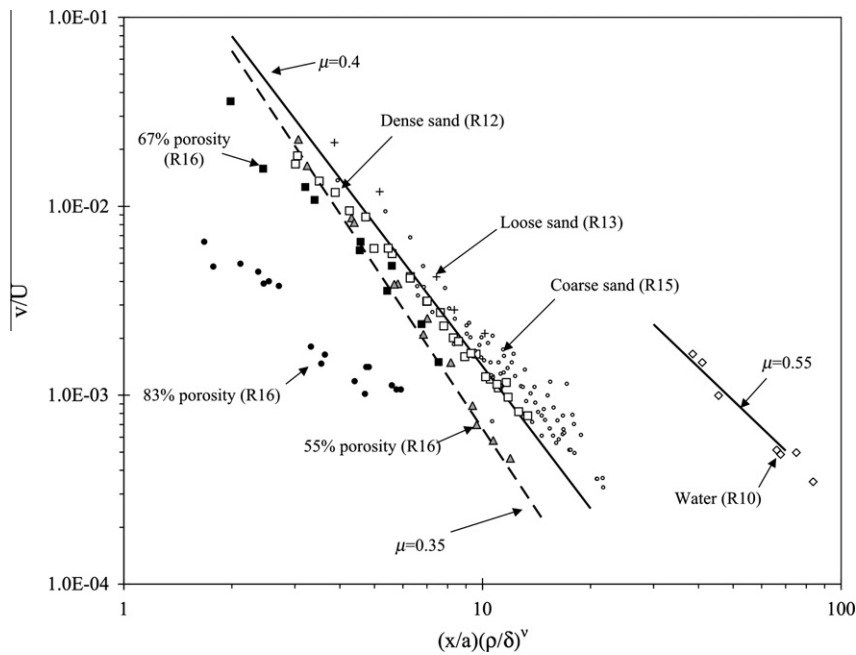

Fig. 11. Ejecta data for water, dry sand and highly porous silicates show how target porosity affects ejection velocities. The projectile energy and momentum are coupled well into low-porosity targets, producing relatively high ejection velocities. Highly porous materials show relatively lower ejecta velocities because of inefficient coupling and significant energy losses as the outgoing shock collapses pore spaces.

and momentum. The data for water follow a slope corresponding to $\mu = 0.55$, which is the same value inferred from measurements of transient crater size in water and final crater size in metals[9] (Holsapple and Schmidt, 1987).

Fig. 12 illustrates the effect of target porosity on the mass of material ejected faster than a given velocity. The data for dense sand, loose sand, and basalt powder all fall on a power-law trend with $\mu \sim 0.4$. Comparison of the results for sand with those for porosities of 55% and 67% shows that $M(v)$ decreases as the porosity of the target material is increased, in agreement with the trend

shown in Fig. 11, i.e. a shift toward lower ejecta velocities as porosity increases. As in Fig. 11, the slope of the data for 55% and 67% porosity is consistent with a value of μ of 0.35.

The data in Fig. 12 for porosities of 70% and 96% are from the centrifuge experiments of Housen and Holsapple (2003). Each centrifuge experiment corresponds to a single data point on this plot, i.e. the total mass of ejecta with speeds sufficient to land on the ejecta collector cloth placed on the target surface (see Section 4.1). Experiments with higher acceleration (G) levels require higher ejection velocities to reach the ejecta collector. Variation in the acceleration level therefore provides data for different ejection velocity values. Collectively, the data show a steady and substantial decrease in ejection velocities as target porosity is increased.

---

[9] Note that the historical expectation that energy scaling with $\mu = 2/3$ should apply for water craters has long ago been put to rest.
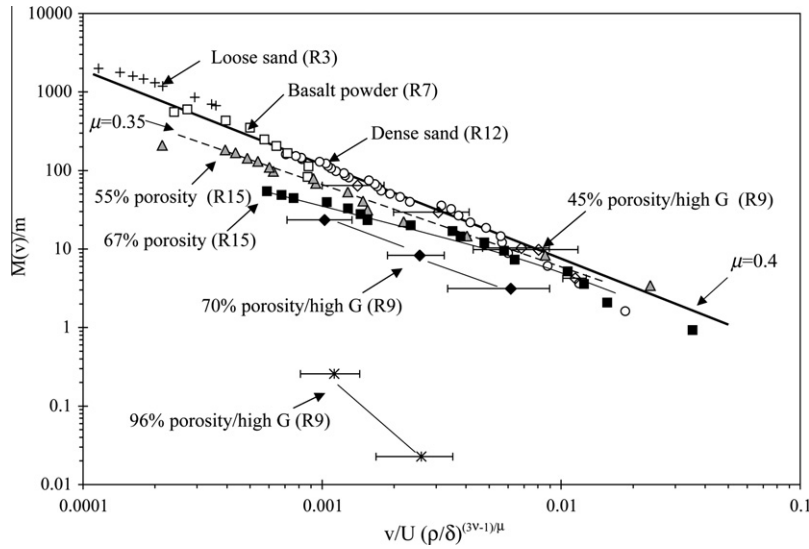
Fig. 12. Data on the mass of material ejected faster than a given velocity illustrate how ejection speeds decrease with increasing target porosity.

6. An ejecta model

In this section, an empirical ejecta model is developed that is consistent with the point-source scaling laws. In principle, one could perform regression fits to the entirety of data and determine scaling laws for all materials including rocks, dense sand, loose sand, micro-spheres, etc. But this would be unwieldy and is not yet warranted by the breadth and quality of the data. Instead, the approach taken here is to broadly sort the data into groups of similar porosity and to provide scaling relationships for each group. Materials with very low porosity such as water or consolidated rock are simply referred to as low porosity and are assigned a value of $\mu = 0.55$ (see Section 3). Various types of granular soils near their maximum packing density usually have moderate porosities in the range of 30–40%. Materials that fall roughly into this category are assigned a value of $\mu = 0.41$. The value of μ for more highly porous materials is currently uncertain. Figs. 11 and 12 indicate a value of $\mu = 0.35$ for target porosities of roughly 60%, which is adopted here. The density exponent, v, is assumed to be 0.4 for all materials (Section 3).

As noted in Section 5.2, experimental studies of ejecta are not presently sufficient to completely illuminate the effects of impact angle. The present model is based on data for vertical impacts and therefore is not expected to apply to cases of significant obliquity. For example, experiments have shown that impacts at 30° to the target surface introduce a significant dependence of ejection velocity on azimuth angle (Anderson et al., 2003; Hermalyn et al., 2008), an effect that is not included here. On the other hand, the results reported by Yamamoto et al. (2006) indicate that impact angle has little effect on the velocity distribution as long as the impact angle is at least 45° from the surface, except for the high-velocity ejecta. Therefore, even though impact angle is not explicitly included here, the present model should apply to cases that are significantly off-normal and especially to the lower speed ejecta.

The ejecta model is developed as follows. Recall that in the gravity regime, Eq. (4) describes ejection velocity as a function of launch position. The argument of the function in Eq. (4) is in terms of x/a, but when written in terms of the crater radius R is actually proportional to x/R, a fact that is easily verified by using the point-source scaling law for crater radius in the gravity regime:

$$R\left(\frac{\rho}{m}\right)^{1/3} = H_1\left(\frac{\rho}{\delta}\right)^{(2+\mu-6v)/[3(2+\mu)]}\left[\frac{ga}{U^2}\right]^{-\mu/(2+\mu)} \tag{10}$$

where H_1 is a constant. Use of Eq. (10) transforms Eq. (4) into the simpler form

$$\frac{v}{U} = \left[\frac{x}{a}\left(\frac{\rho}{\delta}\right)^v\right]^{-1/\mu} f(x/R) \tag{11}$$

In the strength regime, the analog of Eq. (4) is given by

$$\frac{v}{U} = \left[\frac{x}{a}\left(\frac{\rho}{\delta}\right)^v\right]^{-1/\mu} f\left(\frac{x}{a}\left(\frac{Y}{\rho U^2}\right)^{\mu/2}\left(\frac{\rho}{\delta}\right)^v\right) \tag{12}$$

where Y is the target strength. The point-source scaling law for crater radius in the strength regime is

$$R\left(\frac{\rho}{m}\right)^{1/3} = H_2\left(\frac{\rho}{\delta}\right)^{(1-3v)/3}\left[\frac{Y}{\rho U^2}\right]^{-\mu/2} \tag{13}$$

where H_2 is a constant. This can be used to show that the argument inside the function in Eq. (12) is again proportional to x/R. Therefore, Eq. (11) describes the ejection velocity in the strength regime as well as the gravity regime; the effects of strength and gravity are embedded in the crater radius R.

But Eq. (11) needs to be modified for both small and large values of x for the reasons discussed in Section 3. We first discuss the region near the crater edge, where ejection speeds are low. The effects of target strength or gravity cause a departure from the power-law dependence for launch positions near the crater edge. In Fig. 2 this was illustrated as an approach to a vertical asymptote near the edge. This behavior is modeled here by assuming the ejection velocity goes to zero at a distance $x = n_2 R$ and adopting $(1 - x/n_2 R)^p$ for the function f in Eq. (11). That is,

$$\frac{v}{U} = C_1\left[\frac{x}{a}\left(\frac{\rho}{\delta}\right)^v\right]^{-1/\mu}\left(1 - \frac{x}{n_2 R}\right)^p, \quad n_1 a \leqslant x \leqslant n_2 R \tag{14}$$

where the constant n_1 is defined below and the constants n_2 and p are determined by fits to ejection velocity data. That gives a convenient yet simple smoothing between the power-law regime and the vertical asymptote. In the following analysis, separate values of n_2 are allowed for the strength regime ($n_{2,S}$) and the gravity regime ($n_{2,G}$).
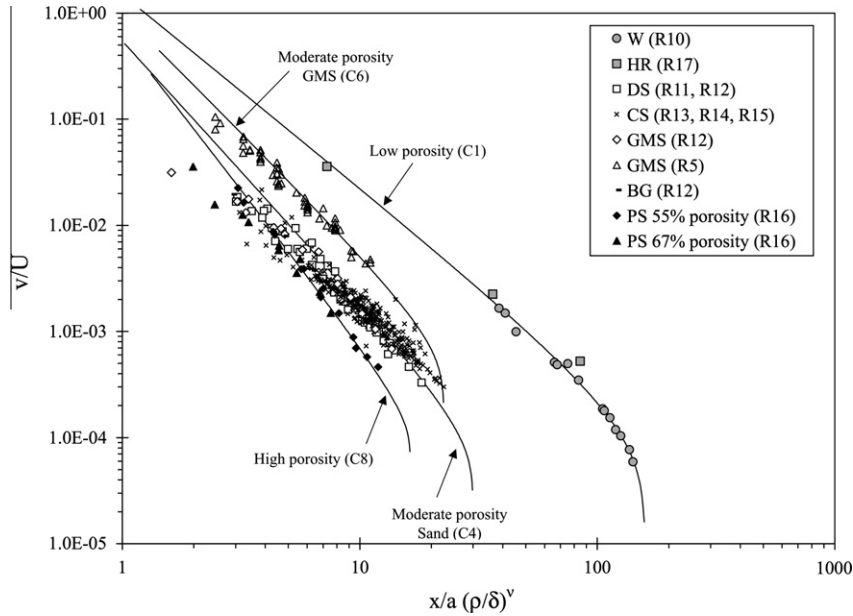
Fig. 13. Comparison of the ejecta model and data for ejection velocity versus position. The results are plotted in the form scaled by the impactor properties. The parameters used to generate the curves are shown in Table 3. The target material codes shown in the legend are: W = water, HR = hard rock, DS = dense sand, CS = coarse sand, GMS = glass micro-spheres, BG = basalt gravel, PS = Perlite/sand mixture.

Richardson et al. (2007) and Collins and Wunnemann (2007) develop a similar empirical form to account for the slowing of the crater radius growth near the crater rim based on a term related to the work against gravity, but do not account for the scaling forms. Since the processes at the termination of crater growth may also be influenced by strength we eschew any motivation based on energy arguments and adopt a simple empirical model consistent with the scaling functional forms.

We also note that the particle velocity in cohesionless materials is non-zero even well outside the crater. For instance, some material is displaced upward to form surface uplift. Also, a thin layer of material near the surface can be launched vertically (albeit at low speeds) by the outgoing shock. While these effects are important when considering processes such as erasure of surface features on small bodies, this material is not considered as ejecta in the classical sense. The present model is designed to apply only to material that is launched from inside the crater.

As discussed in Section 3, the power-law behavior is also not expected to hold for launch positions close to the impact. There is a region near the impact where no ejecta occur because the material is driven downward. In the case of jetting there will be a small region where ejecta are produced, but it will not follow power-law scaling. The current data are insufficient to clarify these details. For the most part, the data for the velocity versus range are well matched by the simple assumption that the power-law curve truncates at a value of $x = n_1 a$, where $n_1 \sim 1.2$, and the power-law holds to that point. That assumption is adopted here, although we note that, given the relative lack of data at high ejection speeds, further work should be done to investigate the high-speed part of the distribution.

A scaling law for the mass, $M(v)$ of ejecta with speed greater than v can be derived from Eq. (14). Because ejection speed decreases monotonically with increasing x, $M(v)$ is equal to the mass, $M(x)$ of material having launch positions less than x, where v is the launch velocity corresponding to position x. This mass is determined by the geometry of the streamlines of the material flow and can be expressed in terms of the point-source measure as

$$M = f(aU^\mu \delta^\nu, \rho, x). \tag{15}$$

The point-source measure is the only quantity involving dimensions of time in this expression and so cannot appear in a dimensionally homogeneous relation. Dropping this quantity leaves a relation between M, ρ, and x; three variables that involve two dimensions (mass and length). As a consequence, they must be related by

$$M = k\rho x^3 \tag{16}$$

where k is a constant. The crater size has an associated mass $M_{crater} = k_{crater}\rho R^3$. Based on an extensive cratering database,[10] k_{crater} is about 0.75 for cohesive soils, in the range of 0.6–0.8 for highly porous materials, and 0.4 for dry sand. If scaled to crater size, Eq. (16) becomes

$$\frac{M}{M_{crater}} = \frac{k}{k_{crater}} \left(\frac{x}{R}\right)^3 \tag{17}$$

At $x = n_2 R$ this ratio must be less than unity, because the total ejecta mass must be less than the crater mass, so the ratio of the two constants cannot be much over unity. In fact, the crater volume is a sum of three parts: the ejected mass, the uplifted mass near the crater rim, and the volume due to compaction. So if compaction and uplift are significant, the value of k/k_{crater} should be distinctly less than unity, perhaps on the order of ½ for common soils and much smaller for highly porous materials. Based on the values of k_{crater} quoted above, this suggests values of k in the range of approximately 0.2–0.4.

Another estimate of k can be made by integrating the volume of material above flow streamlines in a Z-model (Maxwell, 1977). The Z-model is a special case of a point source with $\mu = 1/Z$ (Holsapple and Schmidt, 1987) but with an additional assumption of incompressibility that may not hold for the highly porous cases. Integrations of Z-model streamlines give $k = 0.2$ for a value of $\mu = 0.4$ ($Z = 2.5$), with larger values of k for smaller μ.

Impact experiments by Yamamoto et al. (2005b) verified the relationship in Eq. (16) and give a value of $k = 0.47$ for their glass

---

[10] Available at http://www.keith.aa.washington.edu/craterdata/index.html along with a crater calculation tool.

Table 3
Summary of constants used in ejecta model.

Curve no.	C1	C2	C3	C4	C5	C6	C7	C8
Target	Water	Rock	WCB	Sand	Sand	GMS	SFA	PS
Porosity	~0	~0	20%	35 ± 5%	35 ± 5%	36%	45%	60%
Model of	R10	R1	R2	R15	R3	R4–6	R9	R9
μ	0.55	0.55	0.46	0.41	0.41	0.45	0.4	0.35
C_1	1.5	1.5	0.18	0.55	0.55	1.0	0.55	0.6
k	0.2	0.3	0.3	0.3	0.3	0.5	0.3	0.32
H_1	0.68	–	–	0.59	0.59	0.8	–	–
H_2	–	1.1	0.38	–	–	–	0.4	0.81
$n_{2,G}$	1.5	1.5	–	1.3	1.3	1.3	–	–
$n_{2,S}$	–	1	1	–	–	–	1	1
p	0.5	0.5	0.3	0.3	0.3	0.3	0.3	0.2
a (m)	10^{-3}	1.6×10^{-3}	3.6×10^{-3}	2.4×10^{-3}	3.9×10^{-3}	4.9×10^{-3}	7×10^{-3}	8.7×10^{-3}
U (m/s)	4600	6200	1860	2000	6770	240	1900	1800
δ (kg/m³)	2050	2700	2700	2400	1220	970	930	940
ρ (kg/m³)	1000	3000	2600	1600	1510	1500	1500	1200
Y (MPa)	0	30	0.45	0	0	0	4×10^{-3}	2×10^{-3}

Note: WCB = weakly cemented basalt, GMS = glass micro-spheres, PS = Perlite/sand mixture, SFA = sand/fly ash. All cases shown in this table used: $v = 0.4$, $n_1 = 1.2$, $g = 9.81$ m/s².
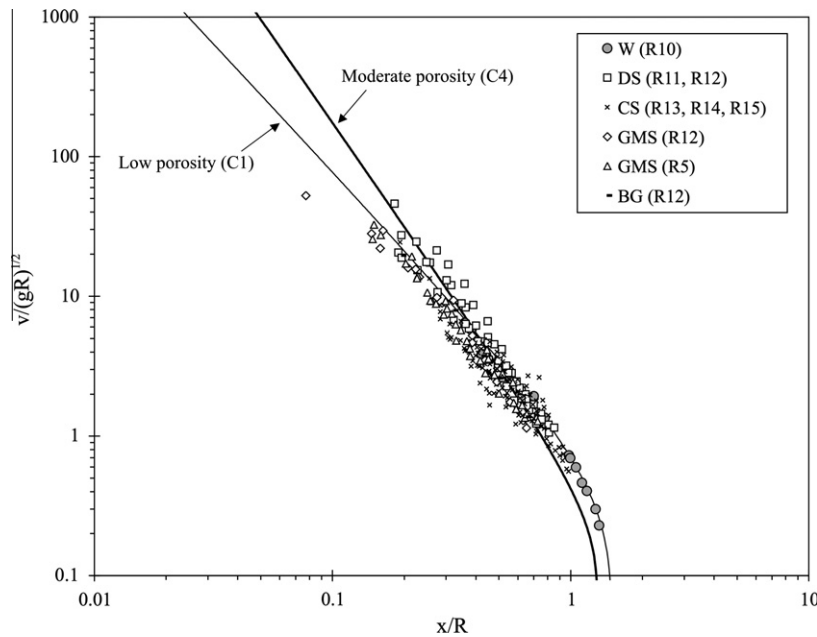

Fig. 14. Comparison of the ejecta model and data for ejection velocity versus position for gravity-dominated impacts. The results are plotted in the form scaled by the crater radius (W = water, DS = dense sand, CS = coarse sand, GMS = glass micro-spheres, BG = basalt gravel).

micro-sphere targets. Direct measurements of k for other materials were not available at the time of this study.

Taken together, the above arguments indicate that k is in the range of 0.2–0.5 for various materials. Using these limits as guides, we estimate k by fitting the ejecta model to laboratory impact data as described below.

Equation (16) must be modified slightly because material inside of $x = n_1a$ is driven downward and not ejected (Section 3). Therefore, $M(x)$ must go to zero at $x = n_1a$. In order to model this behavior, Eq. (16) is replaced by

$$M = k\rho\left(x^3 - [n_1a]^3\right) \tag{18}$$

Returning to the derivation of a scaling law for $M(v)$, for a spherical impactor with mass $m = 4\pi\delta a^3/3$, Eq. (18) is written as

$$\frac{M}{m} = \frac{3k}{4\pi}\frac{\rho}{\delta}\left[\left(\frac{x}{a}\right)^3 - n_1^3\right] \tag{19}$$

Eqs. (14) and (19) form the basis for the ejecta model. Complete distributions for $v(x)$ and $M(v)$ are obtained numerically as follows.[11] Given a set of initial conditions for an event of interest (i.e. g, a, U, ρ, δ, Y), the relevant scaling law (Eqs. (10) and (13)) is used to determine the crater size for the event. Eq. (14) is then used to tabulate ejection velocities for a range of values of the nondimensional launch position x/a. For each value of the launch position, Eq. (19) gives the mass of material launched faster than the corresponding velocity. Example calculations for the ejecta model are now compared to the ejecta data discussed above.

Fig. 13 shows curves generated from the ejecta model for four cases ranging from low to high porosity. Each curve is labeled by a number (e.g. C1, C2, etc.). The parameters used to generate each curve are listed in Table 3. In order to construct the curves, values

---

[11] The power-law portion of the distribution, i.e. for values of x that are large compared to n_1a but small compared to n_2R, can be derived directly from Eqs. (5), (10), (13), and (16). The power-law scaling laws are shown in the lower part of Table 1.

of the parameter C_1 were chosen to pass the power-law portion of the curves through the corresponding data. The constants that determine the approach to a vertical asymptote ($n_{2,S}$, $n_{2,G}$, and p) were selected to fit the data at low ejection speeds when available. The termination of the power-law at high speeds, determined by n_1, is at present uncertain due to a lack of data at high speeds (such measurements are difficult). However, we note that the adopted value of $n_1 = 1.2$ is not inconsistent with the available ejecta data. The constants (H_1 and H_2) shown in Table 3 for the crater size scaling relation were determined from fits to measurements of apparent crater size where available.

Fig. 14 shows the data in the scaling form that involves the crater radius for gravity-dominated cratering. Only the data from gravity-controlled experiments are shown. The curves are based on the ejecta model shown in Eq. (14) and the gravity-regime scaling law for crater radius. It is interesting to note how plotting the ejecta data in terms of crater radius nearly collapses the data for moderately porous materials (e.g. sand) and those for water onto a common trend.

The experiments that used the highly porous Perlite/sand mixtures in Fig. 13 are believed to be strength dominated (Section 4). Therefore, Fig. 15 shows those data plotted in terms of crater
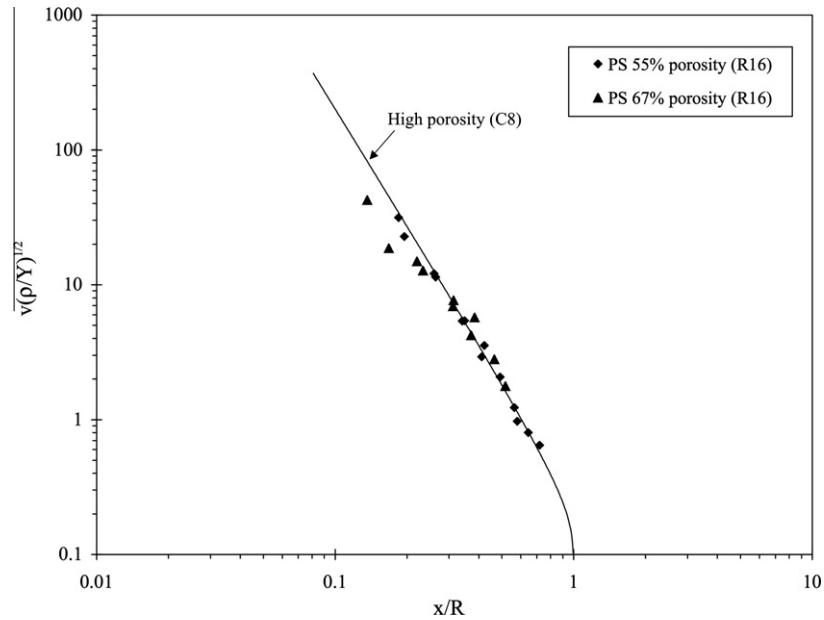

Fig. 15. Comparison of the ejecta model and data for ejection velocity versus position for strength-dominated impacts. The results are plotted in the form scaled by the crater radius (PS = Perlite/sand mixture).
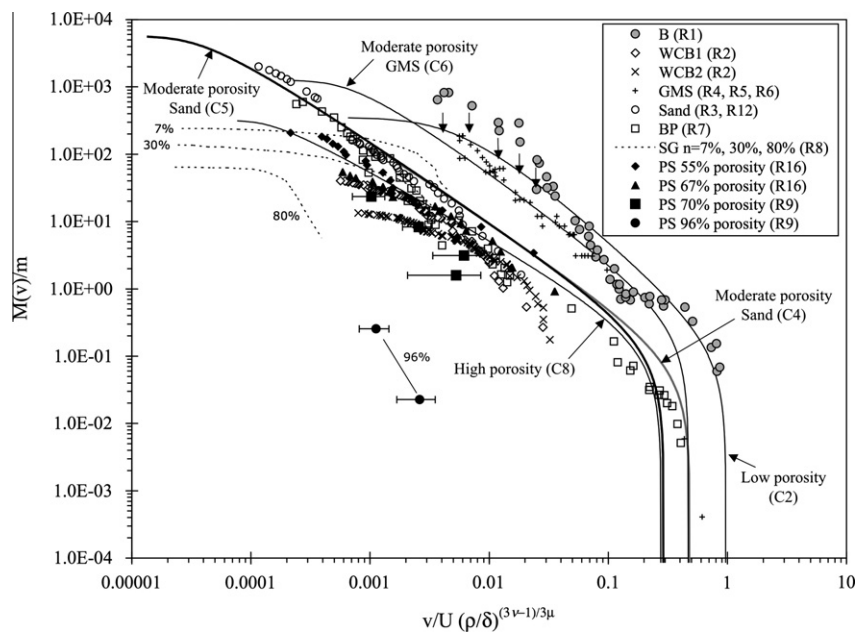

Fig. 16. Comparison of the ejecta model and data for the mass of material ejected with speeds exceeding v. The results are plotted in the form scaled by the impactor properties [B = basalt, WCB1 = weakly cemented basalt ($Y = 0.09$ MPa), WCB2 = weakly cemented basalt ($Y = 0.45$ MPa), GMS = glass micro-spheres, BP = basalt powder, SG = sintered glass beads, PS = Perlite/sand mixture].
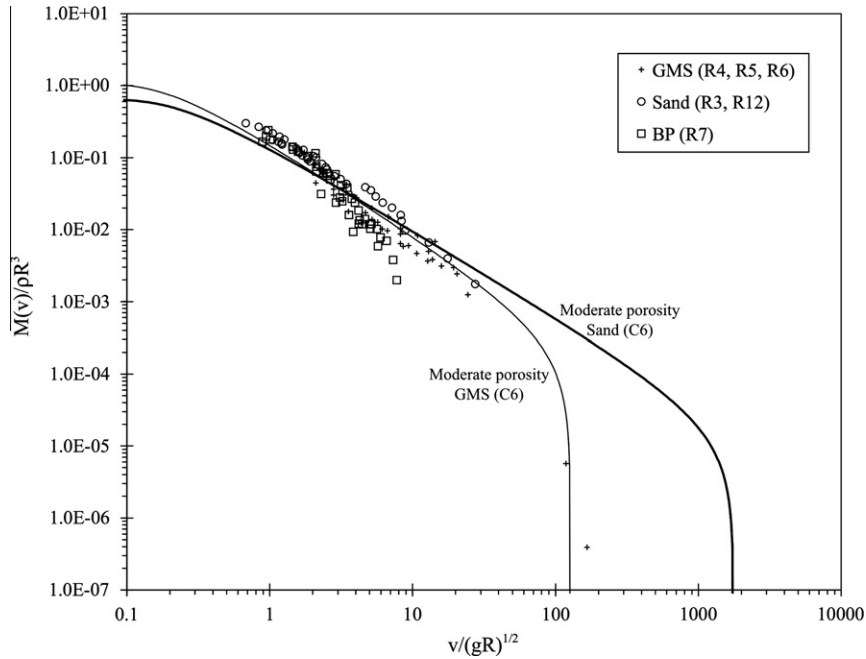
Fig. 17. Comparison of the ejecta model and data for the mass of material ejected with speeds exceeding v for gravity-dominated impacts. The results are plotted in the form scaled by the crater radius (GMS = glass micro-spheres, BP = basalt powder).

radius using the form appropriate for the strength regime. As can be seen, the resulting model curve fits the data in Fig. 15 reasonably well.

Fig. 16 shows the data for $M(v)$ plotted in terms of the impactor properties. The model curves were generated by choosing values of k that made the power-law portions of the curves pass through the data. As shown in Table 3, the resulting values of k are consistent with the values quoted above. Note that the value of k not only determines the y-intercept of the power-law portions of the curves, it also determines the value of the horizontal asymptote, i.e. the total ejecta mass. The value of k that fits the power-law por-

tion of the data also resulted in a horizontal asymptote that is consistent with the data at low ejection speeds. Figs. 17 and 18 show the data and model curves for $M(v)$ in terms of crater size. The crater scaling parameters are shown in Table 3.

The ejecta model, along with the constants given in Table 3, can be used to calculate the ejecta velocity distribution for a given impact event. From those follow a number of important features, including range of ejecta, regolith on small bodies, momentum magnification for asteroid deflection considerations, and so on. Examples of practical applications will be given in subsequent papers.
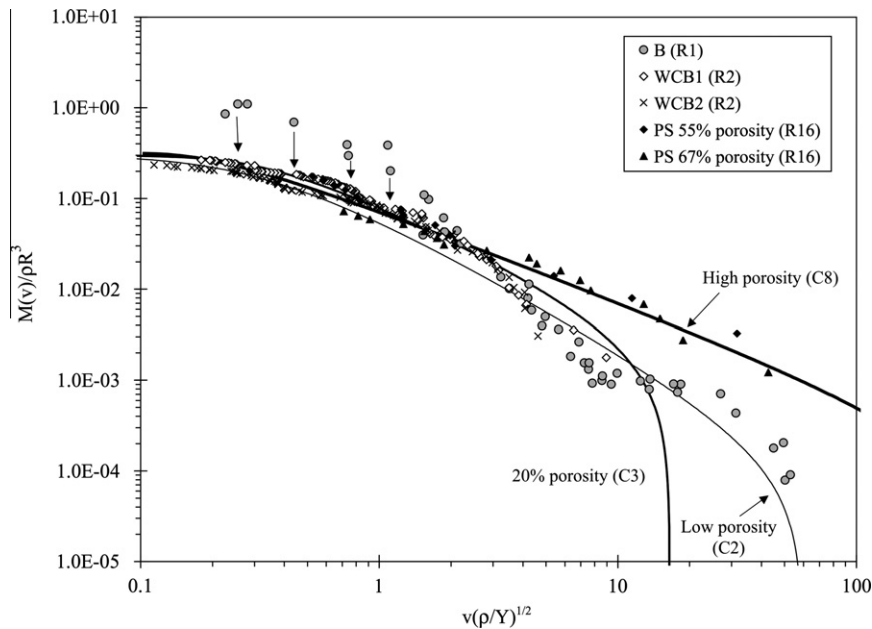

Fig. 18. Comparison of the ejecta model and data for the mass of material ejected with speeds exceeding v for strength-dominated impacts. The results are plotted in the form scaled by the crater radius [B = basalt, WCB1 = weakly cemented basalt ($Y = 0.09$ MPa), WCB2 = weakly cemented basalt ($Y = 0.45$ MPa), PS = Perlite/sand mixture].

7. Conclusions

Ejecta data from the literature and from the authors' own studies were summarized for a variety of target materials. The data, in conjunction with scaling theory, provide significant insights into how the ejecta velocity distribution depends on the conditions of an impact event. As discussed in Section 5, the dependence of ejection velocity on some variables, such as the impactor velocity and density are fairly well understood and follow the behavior expected from scaling theory. The dependences on other variables, primarily the properties of the target material, are only poorly understood. Thus, a number of significant questions remain to be studied.

One of the least understood target properties is material strength. This is in part due to a lack of impact experiments on strength-dominated materials, but also to the fact that strength measurements are often difficult and expensive to perform. This is compounded by a basic lack of understanding of which strength properties (tension, shear, compression) are important and should be measured. Another complication associated with target properties is that the governing strength of many geological materials (certainly rock, but also some cohesive soils) depends on the event size scale.[12] As noted in Section 1, a direct application of laboratory impact experiments in rock would indicate that the surfaces of rocky asteroids smaller than ∼70 km diameter should be essentially barren because nearly all ejecta should exceed the escape velocity; a prediction clearly at odds with observations of asteroid surfaces. A general weakening of rock at large scales undoubtedly results in ejecta velocities much lower than those measured in lab experiments that use pristine targets. A complete ejecta model should include this size effect for rocky materials and will be the subject of a future study. For the present, it is required to pick a strength value representative of the event size in question.

Other target properties need further study as well. For example, it was noted in Section 5.6 that the ejecta velocities measured for glass micro-sphere targets by Yamamoto et al. (2005b) were considerably higher, in a scaled sense, than those of Housen (2011). The most significant difference between those two studies was the impact velocity (one being sub-sonic, the other supersonic). Additionally, there are other studies at relatively low velocities where the general scaling based upon the point-source approach becomes questionable. Thus, further work is required to collect all of the lower speed data under the scaling umbrella.

Target porosity has recently emerged as a fundamental material property with significant effects on the ejecta velocity distribution. Energy losses during compaction of pore spaces cause a reduction in ejection speeds. Under certain conditions identified in Section 7, speeds may be low enough that ejecta do not escape the crater, thus forming a crater without an associated ejecta blanket in the usual sense. Suppression of ejecta blankets requires reduced ejection velocities and crater formation primarily by permanent compaction of the target material. Although this phenomenon has been demonstrated in laboratory experiments (Housen and Holsapple, 2003), it is not completely understood. Does compaction cratering, in which crater size is proportional to impactor size, occur at all size scales in a porous material, or does gravity become important at some size scale? If so, suppression of ejecta would be limited to a range of crater sizes. Does compaction cratering and high target porosity require non-zero cohesion in the target? If so, how much?

The lack of data on the high-speed portion of the ejecta distribution was also noted. Therefore, the parameter n_1 in the present ejecta model is uncertain. Further experimental, and perhaps numerical studies of the high-speed ejecta would be useful.

Much progress has been made in the past two decades in understanding ejecta velocity distributions from impact events. Nevertheless, these crucial questions must be addressed before we can reliably model the impact evolution of planetary bodies or use observations of cratered objects to infer the properties of their surface materials.

References

Anderson, J.L.B., Schultz, P.H., Heineck, J.T., 2003. Asymmetry of ejecta flow during oblique impacts using three-dimensional particle image velocimetry. J. Geophys. Res. 108 E8, 5094. doi:10.1029/2003JE002075.
Anderson, J.L.B., Schultz, P.H., Heineck, J.T., 2004. Experimental ejection angles for oblique impacts: Implications for the subsurface flow-field. Meteorit. Planet. Sci. 39, 303–320.
Anderson, J.L.B., Schultz, P.H., 2005. The effect of projectile density and disruption on the crater excavation flow field. Lunar Planet. Sci. 36. Abstract 1773.
Anderson, J.L.B., Cintala, M.J., Siebenaler, S.A., Barnouin-Jha, O.S., 2007. Ejecta- and size-scaling considerations from impacts of glass projectiles into sand. Lunar Planet. Sci. 38. Abstract 2266.
Andrews, R.J., 1975. Origin and distribution of ejecta from near-surface laboratory-scale cratering experiments. Report AFWL-TR-74-314, 207pp.
Asphaug, E., Ostro, S.J., Hudson, R.S., Scheeres, D.J., Benz, W., 1998. Disruption of kilometer-sized asteroids by energetic collisions. Nature 393, 437–440.
Barnouin-Jha, O.S., Cintala, M.J., Crawford, D.A., 2002. Investigating the effects of shock duration and grain size on ejecta excavation and crater growth. Lunar Planet. Sci. 33. Abstract 1738.
Cintala, M.J., Berthoud, L., Hörz, F., 1999. Ejection-velocity distributions from impacts into coarse-grained sand. Meteorit. Planet. Sci. 34, 605–623.
Collins, G.S., Wunnemann, K., 2007. The effect of porosity and friction on ejection processes: Insight from numerical modeling. Lunar Planetary Institute Contribution 1360, Lunar and Planetary Institute, Houston, pp. 35–36.
Gault, D.E., Wedekind, J.A., 1978. Experimental studies of oblique impact. Lunar Planet. Sci. 9, 3843–3875.
Gault, D.E., Quaide, W.L., Oberbeck, V.R., 1963. Spray ejected from the lunar surface by meteoroid impact. NASA Tech. Note D-1767.
Hartmann, W.K., 1985. Impact experiments. I: Ejecta velocity distributions and related results for regolith targets. Icarus 63, 69–98.
Hermalyn, B., Schultz, P.H., Anderson, J.L.B., Heineck, J.T., 2008. Time-resolved ejecta velocity distribution in oblique impacts. Asteroids, Comets, Meteors 2008, Lunar Planetary Institute Contribution 1405, Paper 8363.
Hermalyn, B., Schultz, P.H., Heineck, J.T., 2009. Early-stage ejecta velocity distribution. Lunar Planet. Sci. 40. Abstract 2492.
Hessen, K.K., Herrick, R.R., Yamamoto, S., Barnouin-Jha, O.S., Sugita, S., Matsui, T., 2007. Low-velocity oblique impact experiments in a vacuum. Lunar Planet Sci. XXXVIII. Abstract 2141.
Holsapple, K.A., 1980. The equivalent depth of burst for impact cratering. Lunar Planet. Sci. XI.
Holsapple, K.A., Schmidt, R.M., 1982. On the scaling of crater dimensions. II – Impact processes. J. Geophys. Res. 87, 1849–1870.
Holsapple, K.A., Schmidt, R.M., 1987. Point-source solutions and coupling parameters in cratering mechanics. J. Geophys. Res. 92, 6350–6376.
Holsapple, K.A., 1993. The scaling of impact processes in planetary sciences. Annu. Rev. Earth Planet. Sci. 21, 333–373.
Holsapple, K.A., 2009. On the "strength" of the small bodies of the Solar System: A review of strength theories and their implementation for analyses of impact disruptions. Planet. Space Sci. 57 (2), 127–141.
Housen, K.R., Schmidt, R.M., Holsapple, K.A., 1983. Crater ejecta scaling laws: Fundamental forms based on dimensional analysis. J. Geophys. Res. 88, 2485–2499.
Housen, K.R., 1992. Crater ejecta velocities for impacts on rocky bodies. Lunar Planet. Sci. 23, 555–556.
Housen, K.R., 2003. Material motions and ejection velocities for impacts in porous targets. Lunar Planet. Sci. XXXIV. Abstract 1300.
Housen, K.R., 2011. Ejecta velocities and flow fields for impacts in porous materials. In preparation.
Housen, K.R., Holsapple, K.A., 2003. Impact cratering on porous asteroids. Icarus 163, 102–119.

---

[12] Either because the target strength inherently depends on size scale (e.g. rocks exhibit many more fractures at large scales than small), or because the strength varies directly with deformation rate, and loading rates decrease with increasing size scale.

Maxwell, D.E., 1977. Simple Z-model of cratering, ejection and the overturned flap. In: Roddy, D.J., Pepin, R.O., Merrill, R.B. (Eds.), Impact and Explosion Cratering. Pergamon Press, pp. 1003–1008.

Michikami, T., Moriguchi, K., Nakamura, R., 2005. Application to large blocks on Asteroid 25143 Itokawa: Ejecta mass distribution with low velocity for impact cratering experiment on porous target. Lunar Planet. Sci. XXXVI. Abstract 1729.

Michikami, T., Moriguchi, K., Abe, M., Hasegawa, S., Fujiwara, A., 2007. Ejecta velocity distribution for impact cratering experiments on porous and low strength targets. Planet. Space Sci. 55, 70–88.

Oberbeck, V.R., Morrison, R.H., 1976. Candidate areas for in situ ancient lunar materials. Proc. Lunar Sci. Conf. 7, 2983–3005.

Perret, W.R., Bass, R.C., 1974. Free Field Ground Motion Induced by Underground Explosions. Sandia National Lab Tech. Report, SAND 74-0252.

Piekutowski, A.J., Andrews, R.J., Swift, H.F., 1977. Studying small-scale explosive cratering phenomena photographically. In: Proc. Int. Congress on High-Speed Photography, vol. 12, pp. 177–183.

Piekutowski, A.J., 1980. Formation of bowl-shaped craters. Proc. Lunar Sci. Conf. 11, 2129–2144.

Richardson, J.E., Melosh, H.J., Lisse, C.M., Carich, B., 2007. A ballistics analysis of the Deep Impact eject plume: Determining Comet Tempel 1's gravity, mass and density. Icarus 190, 357–390.

Richardson, J.E., Melosh, H.J., Artemeiva, N.A., Pierazzo, E., 2005. Impact cratering theory and modeling for the Deep Impact mission: From mission planning to data analysis. Space Sci. Rev. 117, 241–267.

Schmidt, R.M., 1980. Meteor Crater: Energy of formation – Implications of centrifuge scaling. Proc. Lunar Sci. Conf. 11, vol. 3, 2099–2128.

Schmidt, R.M., Housen, K.R., 1987. Some recent advances in the scaling of impact and explosion cratering. Int. J. Impact Eng. 5, 543–560.

Schultz, P.H., Heineck J.T., Anderson, J.L.B., 2000. Using 3-D PIV in laboratory impact experiments. Lunar Planet. Sci. XXXI. Abstract 1902.

Schultz, P.H., Gault, D.E., 1985. Clustered impacts – Experiments and implications. J. Geophys. Res. 90, 3701–3732.

Stöffler, D., Gault, D.E., Wedekind, J., Polkowski, G., 1975. Experimental hypervelocity impact into quartz sand: Distribution and shock metamorphism of ejecta. J. Geophys. Res. 80, 4062–4077.

Sullivan, R.J., Thomas, P.C., Murchie, S.L., Robinson, M.S., 2002. Asteroid geology from Galileo and Near Shoemaker data. In: Bottke, W.F., Jr., Cellino, A., Paolicchi, P., Binzel, R.P. (Eds.), Asteroids III. Univ. Arizona Press, pp. 331–350.

Teramoto, K., Yano, H., 2005. Measurements of sound speed in granular materials simulated regolith. Lunar Planet. Sci. 36. Abstract 1856.

Veverka, J., Thomas, P., Johnson, T.V., Matson, D., Housen, K., 1986. The physical characteristics of satellite surfaces. In: Burns, J.A., Matthews, M.S. (Eds.), Satellites. Univ. Arizona Press, pp. 342–402.

Veverka, J. et al., 1999. NEAR encounter with Asteroid 253 Mathilde: Overview. Icarus 140, 3–16.

Yamamoto, S., Nakamura, A.M., 1997. Velocity measurements of impact ejecta from regolith targets. Icarus 128, 160–170.

Yamamoto, S., Kadono, T., Sugita, S., Matsui, T., 2005a. Velocity distributions of high-velocity ejecta from regolith targets. Icarus 178, 264–273.

Yamamoto, S., Okabe, N., Sugita, S., Matsui, T., 2005b. Measurements of ejecta velocity distribution by a high-speed video camera. Lunar Planet. Sci. XXXVI. Abstract 1600.

Yamamoto, S., Kadono, T., Sugita, S., Matsui, T., 2006. Cumulative mass-velocity distribution of impact ejecta in oblique impacts. Lunar Planet. Sci. XXXVII. Abstract 1164.

Yang, W., Ahrens, T.J., 1995. Impact jetting of geological materials. Icarus 116 (2), 269–274.